minerals

MDPI

Article

World-Class PGE-Cu-Ni Talnakh Deposit: New Data on the Structure and Unique Mineralization of the South-Western Branch

Nadezhda Krivolutskaya [1,*], Nadezhda Tolstykh [2], Tatyana Kedrovskaya [3], Konstantin Naumov [4], Irina Kubrakova [1], Oksana Tyutyunnik [1], Bronislav Gongalsky [5], Elena Kovalchuk [5], Larisa Magazina [5], Yana Bychkova [6] and Anton Yakushev [5]

1 Vernadsky Institute of Geochemistry and Analytical Chemistry, Russian Academy of Sciences, Kosygin St., 19, 119991 Moscow, Russia; i_kubrakova@mail.ru (I.K.); toa-6767@mail.ru (O.T.)
2 V.S.Sobolev Institute of Geology and Mineralogy, Siberian Branch of Russian Academy of Sciences, Koptyuga Ave., 3, 630090 Novosibirsk, Russia; tolst@igm.nsc.ru
3 Russian Federal Geological Foundation, 3d Magistralnaya St., 38, 125993 Moscow, Russia; shlychkova.tanya@yandex.ru
4 MMCo Norilsk Nickel, Polar Division, Lenina Ave., 1, 663300 Norilsk, Russia; tiptur13@mail.ru
5 Institute Geology of Ore Deposits, Petrography, Mineralogy and Geochemistry, Russian Academy of Sciences, Staromonetny Per., 35, 119017 Moscow, Russia; brgon@mail.ru (B.G.); elena7kovalchuk@gmail.com (E.K.); lm@igem.ru (L.M.); antemp@inbox.ru (A.Y.)
6 Lomonosov Moscow State University, Leninsky Gory, 1, 119992 Moscow, Russia; yanab66@yandex.ru
* Correspondence: nakriv@mail.ru; Tel.: +7-926-543-4787

Received: 30 December 2017; Accepted: 15 March 2018; Published: 21 March 2018

Abstract: The Talnakh deposit is one of the largest PGE-Cu-Ni deposits in the world. It is located inside the North-Western part of the Siberian Trap province and consists of three branches. The problem of massive ore origins has been discussed for several decades. The structure of the South-Western branch and the mineralogy of related its Cu-rich ore are discussed in this article. The Southern-2 orebody has a deep inclination (45°) inside the intrusive body, close to its wall, in contrary to the horizontal orebodies of the North-Eastern branch. Mineral composition of the Southern-2 orebody differs from the composition the other orebodies of the Talnakh intrusion as well. It consists ofchalcopyrite, pentlandite with subordinate cubanite, and pyrrhotite. Its specific feature is a large amount of bornite and chalcocite. These minerals occur in disseminated and massive ores. The ores of the other branches of the Talnakh intrusion have chalcopyrite-pyrrhotite compositions whilethe Southern-2 massive ore is enriched in Cu (19.03–25.8 wt %; Cu/Ni = 3.8–8.6) and PGE: ΣPGE changes from 39.1 to 279 ppm, Pd/Pt = 1.3–32. Twelve minerals of the systems Pd-Sn-Cu, Pd-Pb-Bi, Pd-Ni-As, Au-Ag-Pd-Cu, and intermetallics of the Pt-Fe-Cu-Ni types were discovered in ores, but are also widespread in other orebodies. Isoferroplatinum, sperrilite and cooperitewere not found. The unusual structure and composition of the Southern-2 orebody suggest its origin from a separate magma impulse. The correlation between disseminated and massive ores of the Southern 2 orebody in term of chemical and mineralogical composition is evidence of the formation of massive oresin situ, without displacement along the bottom of the massif.

Keywords: Norilsk area; PGE-Cu-Ni ores; gabbro-dolerites; Talnakh; massive ore origin

1. Introduction

The North Siberian Platform is a large metallogenic province including numerous PGE-Cu-Ni deposits. Three of them are huge sulfide deposits located in the Norilsk area: The Oktyabr'skoe, Talnakh, and Norilsk 1. They have been described in many publications [1–35].

These deposits have some specific features compared with the other Cu-Ni and PGE deposits. First of all, they are related to mafic-ultramafic intrusions located in the north-western part of the Siberian Trap province (251 ± 0.3) [36,37] (Figure 1: Schema of the geological structure of the Norilsk area), while the other deposits relate to the large Proterozoic plutons. As a result, massive sulfide orebodies (average thickness is 20–30 m, maximum is 56 m) in the Norilsk area are associatedwith thin gabbro-dolerites intrusions (150 m in thickness). This geological positioning of orebodies poses a question about the mechanism of their formation.

Many models of ore formation have been created since their discovery at the beginning of the twentieth century. They include magmatic, metasomatic, and pneumatholithic processes of ore origin [2,10–12,16–19,24,30]. Magmatic hypothesis are considering two versions of ore origin: within the closed magmatic system [2,4–8,18,19,23,26,29,38] and the open magmatic system [21,39–42]). In both models the mechanism of formation of massive orebodies is debatable. Some researchers believe that the ores form by filter-pressing of sulfide melts from the intrusion into the country sediments [6]. Others suggest that those ores can be derived by emplacement of a sulfide melt [18,19,43].

To solve the problem of the mechanism of massive ore formation it is necessary to study the mineral compositions of massive and disseminated ores together. In most cases a comparison of these two ore types does not give a result because they have ordinary compositions of pentlandite-chalcopyrite-pyrrhotite. Only one orebody is described in the literature in detail [18,43–49] had unusual composition. It is the Octyabr'skoe deposit (2 km × 4 km × 0.05 km) hosted by the Kharaelakh intrusion which has been completely explored recently. The mineral zoning from the center to the contact has been described as talnakhite-cubanite-chalcopyrite-pyrrhotite ore types. The Octyabr'skoe deposit is characterized by mineralogical diversity, large quantities and size of many rare minerals, especially platinum group minerals discovered here for the first time: Talnakhite, putoranite, sobolevskite etc. [50–62]. Nevertheless, the outer zone of this orebody consists of pyrrhotite, and disseminated ore in gabbro-dolerites has the same composition. This very common composition does not allow us to determine their origin.

However, there are a few other orebodies that have unusual chemical and mineralogical composition and that have never been studied and described before. These are orebodies of the Southern part of the Talnakh deposit. We present mineralogical and geochemical data on the Southern 2 orebody of the Talnakh intrusion which is rich in Cu and PGE. Comparison of compositions of disseminated and massive ore demonstrates their similarity, suggesting their formation by a filter-pressing process in situ, without essential movement of sulfide melt along the bottom of the gabbro-dolerite massif. In short, they were crystallized from separate impulse of the silicate melt which formed the Southern branch of the Taknakh intrusion. The Norilsk-Kharaelakh Fault played an essential role in the localization of the intrusive and ore bodies that is proved by the structure of this block of the Talnakh deposit.

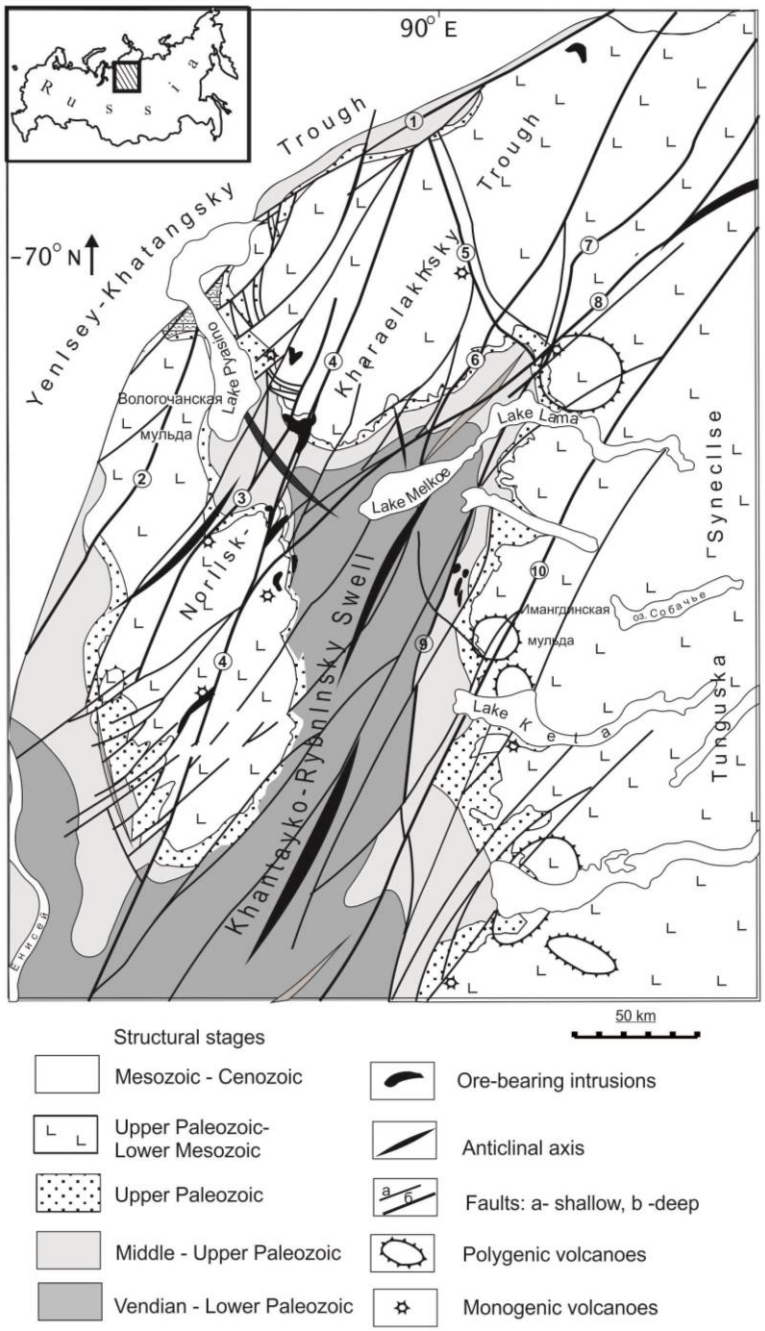

Figure 1. Tectonic schema of the Norilsk area (constructed by Mikhailov and authors based on a geological map of the Norilsk area [62]). Faults, number: 1—North-Kharaelaksky, 2—Pysinsky, 3—Daldykansky, 4—Norilsk-Kharaelakhsky, 5—Kumginsky, 6—Neralakhsky, 7—Abagalakhsky, 8—Mikchangdinsky, 9—Imangdinsky-Letninsky, 10—Keta-Irbinsky.

2. Brief Description of the Geology of the Norilsk Area and the Talnakh Intrusion

2.1. General Characteristic of the Area

The Norilsk area is located North of the Siberian platform (Figure 1)consists of huge sequences (7–10 km) of carbonate-terrigenouse rocks (Rhiphae-Devonian) with interlayers of gypsum, anhydrite and salt [63]. They are covered by coal-bearing sandstones and siltstones, combined in the Tunguska Group rocks (C_2–P_3). Thicknesses of basalts and tuffs of the Siberian Trap formation covering terrigenous rocks reaches up 3,5 km. Its age was estimated as 251 Ma [36,37]. Volcanic rocks were subdivided into 11 formations [64], the three lower onesare subalkaline with elevated TiO_2 content (up to 3.5 wt %) and high Gd/Yb ratio while upper formations have a typical tholeiitic

composition with TiO_2 around 1wt %. Numerous basic-ultrabasic intrusions coeval to lavas are located mostly in the Devonian and Tunguska Group rocks. Their morphology vary from sill-like to irregular bodies.

2.2. Deep Structure of the Area

The Norilsk region is located within the Norilsk megablock, which is restricted by the Yeniseysky, Malokhetsky and Keta-Irbinsky faults (respectively in the North, West and East). The last one separates the Norilsk megablock from the megablock corresponding to the Tunguska syneclise (Figure 1). The increased permeability of the earth's crust here is determined by the development of a long-lived rift system associated with the Yenisey-Khatangsky Ttrough (the Norilsk-Kharaelyakhsky Trough). The Eastern part of the area refers to the Tunguska syneclise. The latter is separated from the Norilsk-Kharaelyakhsky Trough by the Khantaysko-Rybninsky Swell. The formation of the Norilsk-Kharaelakhsky Trough began in the Late Paleozoic time, the maximum development occurred in the Permo-Triassic volcanic activity, and the final structural appearance was acquired during the post-volcanic period, when anticlines were formed. The permeability of the earth's crust in the extreme North-West of the platform is associated with the development of intracontinental rift structures of the West Siberian plate and the Yeniseysko-Khatangsky Troughs. All known Cu-Ni deposits of the Siberian Platform are located here. The surface of the crystalline basement within the central part of the Kharaelakhsky Trough lies at a depth of 7–8 km and rises to the Southern and South-Eastern directions to 5 km.

2.3. The Position of the Intrusions

Differentiated intrusions are combined into the Norilsk Intrusive Complex, three of them contain enormous sulfide contents forming the Oktyabr'skoe, Talnakh and Norilsk 1 deposits located inside two ore junctions, the Norilsk and Talnakh (Figure 1). The last one comprises the Oktyabr'skoe and Talnakh deposits. It is believed [9,10,18], that the Norilsk-Kharaelakh Fault (NKF) determined the position of these ore-bearing massifs located at different levels of the rock sequence.

The localization of the differentiated intrusions of the Talnakh ore junction shows a "branching bundle" [65] relative to the Norilsk-Kharaelakhsky Fault (NKF) (Figure 2). Intrusive bodies occur in the deep regions (around 500 m from the surface) and rise to the modern surface. It is important to emphasize that they do not reach the lava flows.The Talnakh intrusion is elongated in the meridian direction at around 20 km [7,9,65,66].

The intrusion's width is 1 km and the average thickness is 150 m. The roof is flat while the bottom is undulated, with many dips. It lies at a slight angle with respect to the host rocks of the Devonian and the Tunguska rock group. The Talnakh intrusion consists of two branches, South-Western and North-Eastern, separated by Norilsk-Kharaelakh and feathering faults. Some authors [38,65] also distinguish the North-Westernbranch (Figure 2, we follow this classification), sometimes referred to as the Kharaelakh intrusion. The connection of these branches is complex, because this area is broken by a series of discontinuous faults and fractures, in which displacements of up to 0.3 km are observed. The North-Eastern branch is located to East of the main NKF, with a shallow dip (5–6 degrees) to the North-East. Its length is more than 10 km, width is 1200 m, and the maximum thickness is 250 m. The South-Western branch is elongated along the NKF for 6 km and dips to the North-Eastat an angle of 4°–6°. The bottom has a keel-shaped chute. The North-Western branch is isometric and is located to the West of the NHF (Figure 2).

The internal structure of the Talnakh intrusion is typical of other ore-bearing intrusions of the Norilsk Intrusive Complex. It consists of gabbro-dolerites (from bottom to top): contactic, taxitic, picritic, olivine, olivine-bearing, olivine-free (we follow the nomenclature of rocks adopted to the Norilsk area and used by geologists for several decades) [4,9,13,38]. The upper zone of intrusions comprises gabbro-diorites, leucogabbro, upper picritic and taxitic gabbro-golerites and magmatic breccias. Some horizons can be absent in this zone.

There are four types of sulfide ores related to the Talnakh intrusion: (i) disseminated pentlandite-chalcopyrite-pyrrhotite ore in the taxitic and picritic gabbro-dolerites; (ii) massive pentlandite-

chalcopyrite-pyrrhotite ore in the lower contact zone of massif and surrounding rocks; (iii) disseminated chalcopyrite ore in surrounding rocks; and (iv) low-sulfide ore in upper zone of massifs (in the upper taxitic, picritic gabbro-dolerites and leucogabbro). As a rule the massive ores are concentrated close to the bottom of the intrusion, in several centimeters to several meters away from the contact in the Devonian carbonate-terrigenous sedimentary country rocks or in the Tunguska Group. They occupy a horizontal position and are related to troughs in the bottom of the intrusion [5,6]. However, these geological features are typical only for North-Eastern part of the deposit.

All these types are enriched in PGE compared with other Cu-Ni deposits in the world. Many publications are devoted to the North-Eastern part of the Talnakh deposits [7,9,38,66–69] and the Kharaelakh intrusion [6] but there is little data on the South-Western part deposit and absolutely none about related ores. This is the first description of Cu-rich ore in the South-Western branch. Furthermore, the study of the structure and composition of intrusions and ores allows one to answer a number of questions related to the mechanisms of formation of deposits.

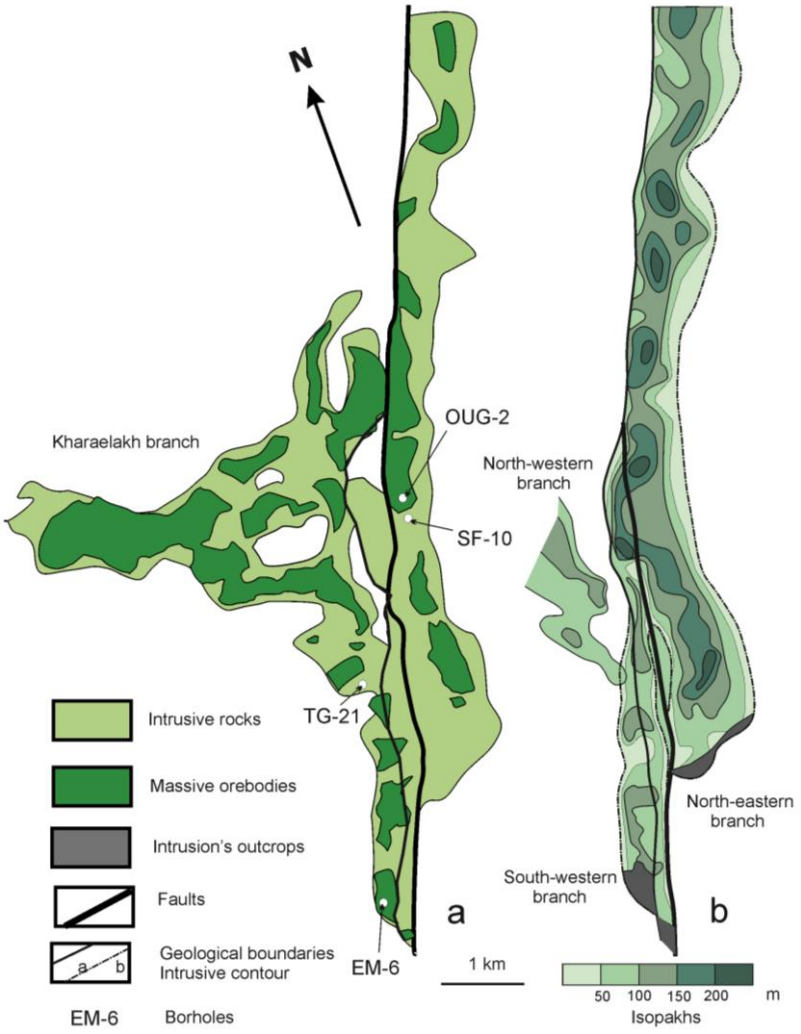

Figure 2. Position of the orebodies (**a**) (after Natorkhin et al., Turovtsev [65,66]). Projection on the surface; (**b**) (after Geology of Ore Deposits [69]) and isopach map of the Talnakh intrusion with studied boreholes.

3. Materials and Methods

We have studied the Southern 2 orebody of the Talnakh deposit located in the South-Western branch (enriched in Cu and PGE) in detail and compared their intrusive rocks and ores with North-Eastern (boreholes OUG-2 and SF-10) and South-Western branches (borehole TG-21).

The South-Western portion of the Talnakh deposit is characterized based on data from the core material recovered by the borehole EM-6, which penetrated the Southern 2 orebody and the samples collected in the underground mine "Majak" (samples MA-12a–MA-17a).

Major elements in the rocks were analyzed by XRF method at the Institute Geology of Ore Deposits, Petrography, Mineralogy and Geochemistry RAS (IGEM RAS), by analyst A.I. Yakushev. Determination of the concentration was done with Wavelength Dispersive X-ray Spectrometer, model Axios mAX production company PANalytical (Eindhoven, The Netherlands). The spectrometer is equipped with X-ray tube with a capacity of 4 kW Rh-anode. The maximum rated tube voltage 60 kV max anode current of 160 mA. Eleven elements were measured, and the relative standard deviation for the majority of these elements was between 1.2% and 4.5% (relative standard error of 5.6% for TiO_2 and 13% for Cr_2O_3); detection limits are given in Table 1, No. 24. Quality control of the results of the analysis performed on standard samples of rocks U.S. Geological survey (USGS) BCR-2, DTS-2, BHVO-1 (Table 1, No. 25–30).

Analysis of rare elements in rocks was carried out by ICP-MS (Element-2, Thermo Scientific, Darmstadt, Germany) at Lomonosov Moscow State University by Ya.V. Bychkova. The detection limits of elements were from 0.1 ppm for elements of heavy and intermediate atomic weight to 1 ppm for light elements (Table 2, No. 10). The accuracy of the analyses was 1%–3%. The standards were certified samples BHVO-2 and COQ-(Table 2, No. 11–12).

Base and precious metals were analyzed at the Laboratory of the Geochemistry and Analytical Chemistry of Precious Metals at the Vernadsky Institute (analysts I.V. Kubrakova and O.A. Tyutyunnik). To analyze ore samples, they were decomposed by heating with a mixture of concentrated HF + HNO_3 and then dried to wet salts. The salts were treated with reverse aqua regia (HNO_3:HCl = 3:1) to the complete oxidation of the elemental sulfur, and wet salts were then obtained. Upon complete dissolution of the salts, the solution was cooled and filtered into a 100 mL flask. The filter with precipitate was placed in a corundum crucible, ashed in a muffle furnace at 500 °C, fused with a double-excess quantity of Na_2O_2 at 600 °C and then treated with HCl to convert the salts into chlorides. The solution obtained was mixed with filtrate. To analyze Au, Pt, Pd, and Rh, a preconcentration of noble metals on a complex-forming sorbent POLYORGS IV was performed; the sorbent as a suspension was analyzed by ETAAS on a Solaar MQZ (Thermo Electron Corp., Cambridge, UK) at 242.8, 265.9, 247.6, and 343.5 nm, respectively. Silver was analyzed in the initial solution by ETAAS at 328.1 nm with 1.25% ascorbic acid as a modifier. Fe, Cu, Ni, Co, and S were analyzed by ICP-AES on an Iris Intrepid II XDL (Thermo Electron Corp., Franklin, MA, USA). The accuracy of the determination was confirmed by replicated analysis of SRMs SARM-7B (Platinum ore) and KN-1 (Nickel concentrate).

Minerals were analyzed using a CAMECA SX 100 (Cameca, Gennevilliers, France) at the Vernadsky Institute of Geochemistry and Analytical Chemistry (analyst N.N. Kononkova) and JEOL JXA 8200 SuperProbe (3-1-2 Musashino, Akishima, Tokyo 196-8558, Japan) at IGEM RAS (analyst E.V. Kovalchuk) at 40 nA beam current and 20 kV accelerating voltage; the counting times were 10 s when major components were analyzed and 20s for trace elements. Back-scattered electrons images BSE images were taken on an Jeol JSM-6480LV electron microscope (Jeol, Tokyo, Japan) at the Institute Geology of Ore Deposits, Petrography, Mineralogy and Geochemistry RAS Laboratory of Analytical Techniques (beam current 10 nA, accelerating voltage 20 kV, live counting time 100 s; analyst L.O. Magazina) and by scanning electron microscope (SEM) a LEO 1413 VP equipped by an energy dispersive spectrometer (EDS) with spectrometer (EDS) "Oxford" at the V.S. Sobolev Institute of Geology and Mineralogy.

4. Results

4.1. Morphology of the Branches of the Talnakh Intrusion

Based on the data of isohypses and isopaches maps [65,66] and the drilling results of Norilskgeologiya Ltd., we constructed several sections through the massif that help get additional information about the morphology of their branches (Figure 3). According to these data, the North-

Eastern branch is a ribbon-like body. The intrusion plunges to the North-East at a steeper angle than the surrounding rocks which fall in the same direction. Thus, its Southern part (partially eroded) lies in the deposits of the Tunguska Group, while the Northern part is located in the Upper Devonian rocks (the Kalargonsky Formation). The intrusion's bottom is uneven, which results in a narrowing of the cross section of the intrusion [8]. The massive ores have a subhorizontal position in the section. As a rule, they are localized in a few decimeters from the lower intrusive contact, while the transition from disseminated ores to massive ones at the base of the intrusion occurs gradually. Sulfides gradually penetrate into the host rocks and accumulate in the form of large (up to 40 m, borehole OUG-2 [23]) or small (first decimeters, borehole SF-10, TG-21) orebodies.

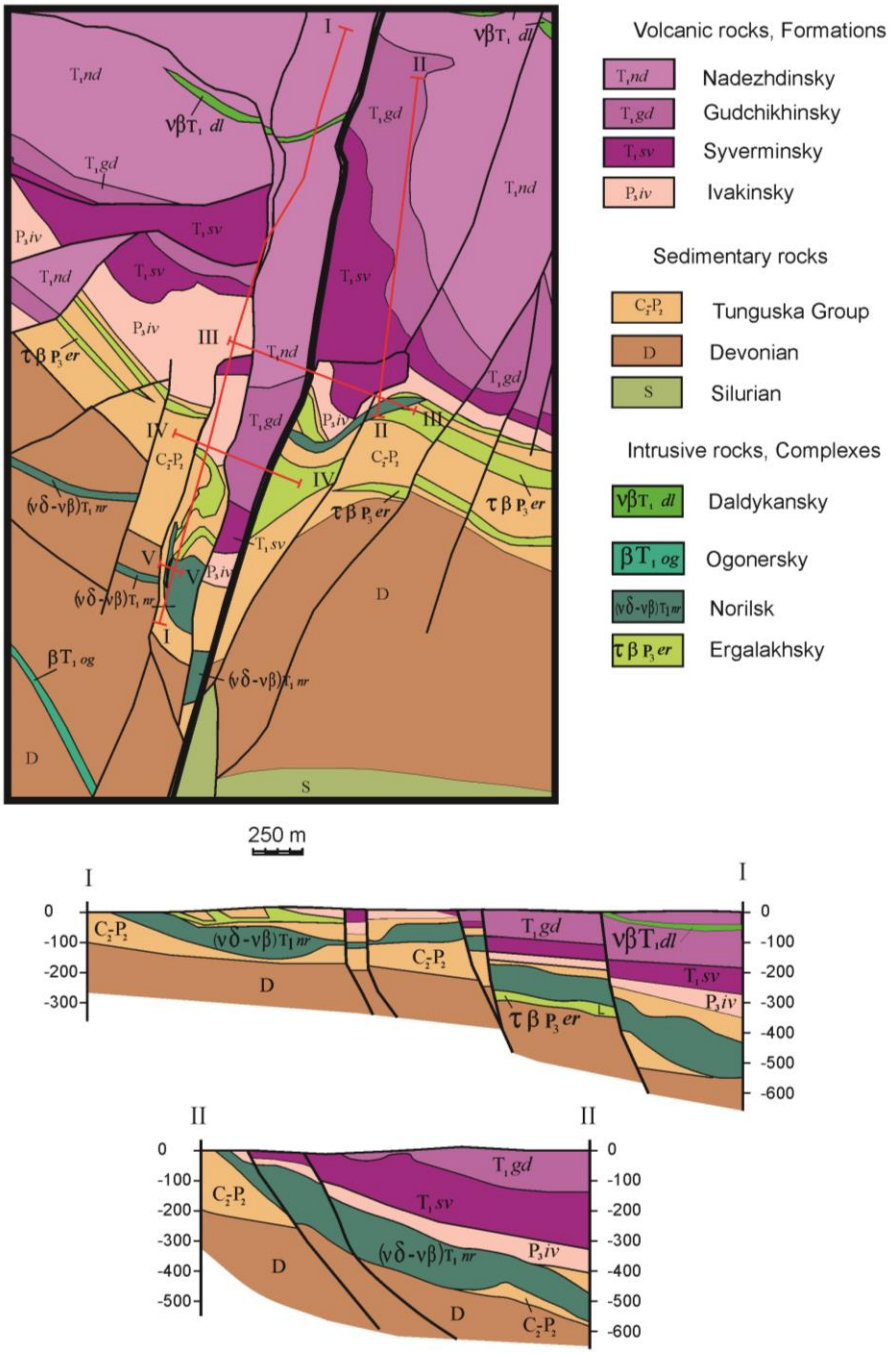

Figure 3. Geological map of the Talnakh ore junction and cross-sections I-I and II-II (here and in Figure 4 based on data of Ltd. Norilskgeologia with author's corrections) with the longitude sections. The red lines on the map are line of cross section and their numbers.

The morphology of the South-Western part of the Talnakh intrusion substantially differs from those described above. The intrusive body is localized in a graben-shaped block displaced 250 m to the South and formed by two branches of the NCF [8,65], the planes of which restricted the distributionof magma flow to the West and to East. As a result, the sides of the intrusion have a steep fall to the central part, caused by the steeply falling planes of tectonic disturbances (Figures 3 and 4). The Southern parts of the South-Western and North-Eastern branches are eroded. The Talnakh intrusion is submerged to the North-East, with a slight uplift in the center. The Southern part of it lies in the Tunguska Group of rocks, while the Northern part is located in the Devonian rocks. In the North, according to [65], the intrusion connects with the North-Eastern and North-Western parts by thin conductors at a depth of about 500 m from the surface.

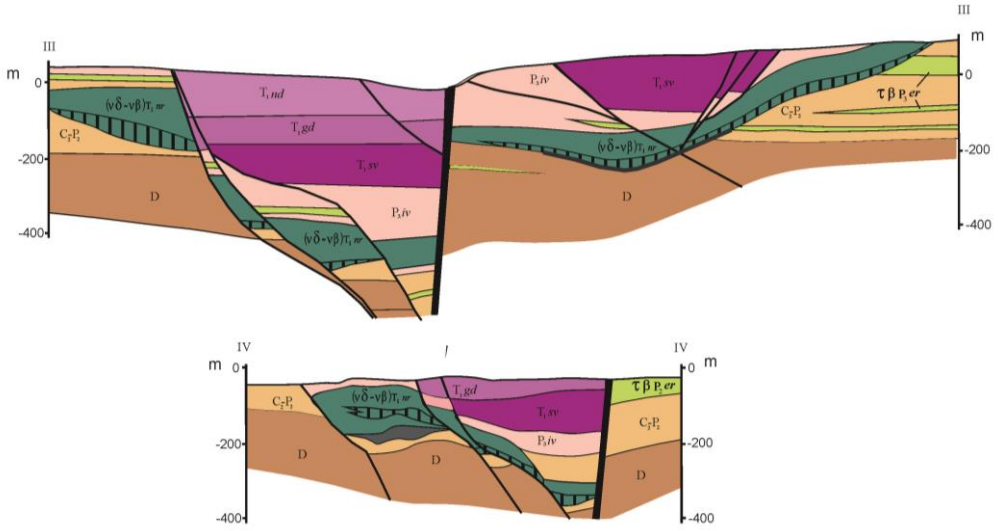

Figure 4. Cross-sections III-III and IV-IV of the Talnakh branches (based on authors data and after Likhachev [5]). Captions in Figure 3.

4.2. Internal Structure of the Intrusive Branches

The above alternation of rock varieties in the section of intrusions is preserved, but horizons thicknesses vary considerably, especially in the case of picritic gabbro-dolerites and gabbro-diorites. The section of the North-Eastern branch is represented (with a total thickness of 118 m, borehole SF-10, Figure 5a) by different gabbro-dolerites (contactic, taxitic, picritic, olivine, olivine-bearing, olivine-free) and gabbro-diorite (Table 1). In the upper part, thin horizons of picritic and taxitic gabbro-dolerites are observed with elevated Cu and Ni contents (Table 1) as well as magmatic breccias with fragments of coals and cemented gabbro material. The most distinct variations in the composition of rocks are reflected in the distribution of MgO (Figure 5, Table 1), the content of which sharply increases in picritic gabbro-dolerites (both in the lower part of the section and in the upper section). However, massive ores are practically absent in the section because the borehole is drilled behind the contour of rich economically valuable ores.

An analogous structure of the section is observed in the previously described section in OUG-2 borehole [23], which penetrated 40 m into massive ores. The thickness of the horizon with disseminated ores reaches 27 m. The difference in the structure of the intrusive part of these sections (Figure 5a,b) is in the absence of upper picritic horizons and magmatic breccias in the borehole OUG-2.

The North-Western branch (borehole TG-21) is distinguished by the increased capacity of the taxitic gabbro-dolerites (Figure 5c). Thus, the total thickness of picritic and taxitic gabbro-dolerites, as well as partly ore-bearing olivine gabbros, forming a productive horizon of economicallyvaluable mineralization, reaches almost 50 m. The thickness of massive ore is around 1 m.

These branches have similar composition in rare element distributions reflected in spider-diagrams (Figure 6, Table 2).

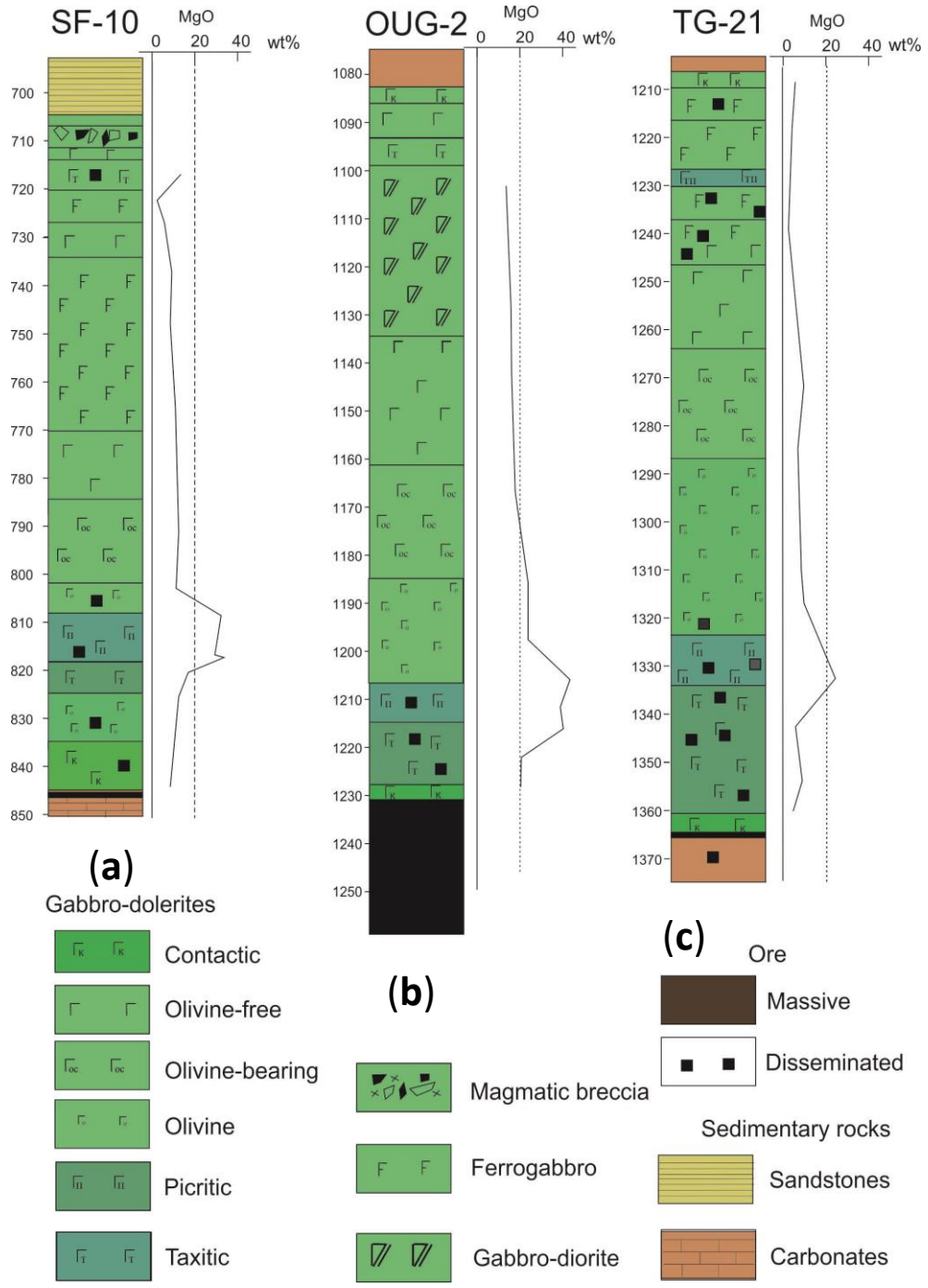

Figure 5. Internal structure of the intrusive branches and MgO distribution in the sections.Boreholes SF-10 (**a**), OUG-2—North-Eastern branch (**b**), TG-21—South-Western branch +MgO (**c**). Data in Table 1 (SF-10) and (after [23] for OUG-2 and after [34] for TG-21).

Table 1. Chemical composition of the rocks from the Talnakh intrusion, wt %.

No.	1	2	3	4	5	6	7	8	9	10
Depth, m	727.4	730.2	731.1	732.5	737.8	746.5	756.6	759	761.5	773.8
SiO_2	43.7	49.9	50.9	57.8	49.4	50.4	49.5	48.3	49.3	48.7
TiO_2	0.46	1.37	1.71	1.20	1.63	1.01	1.16	1.09	1.02	0.90
Al_2O_3	16.1	13.0	13.5	13.8	13.4	13.3	14.4	15.1	15.4	15.2
FeO tot.	10.3	11.8	12.6	8.7	12.3	10.1	11.5	10.3	10.5	9.3
MnO	0.14	0.14	0.14	0.09	0.16	0.20	0.21	0.19	0.19	0.16
MgO	12.0	6.6	4.2	2.3	5.9	7.8	6.8	7.4	7.6	9.1
CaO	8.3	10.6	9.9	6.0	11.0	11.5	10.5	11.3	11.3	12.6
Na_2O	0.8	3.3	3.7	7.6	3.1	2.5	2.7	2.7	2.1	1.9

K_2O	2.1	1.0	1.2	0.2	0.8	1.2	0.9	0.9	0.8	0.6
P_2O_5	0.07	0.16	0.21	0.42	0.16	0.11	0.13	0.12	0.12	0.10
Cr_2O_3	0.43	0.04	0.01	0.01	0.02	0.05	0.10	0.07	0.07	0.19
LOI	4.80	1.83	1.48	1.41	1.83	1.65	1.89	2.26	1.39	1.02
S	0.6	0.3	0.3	0.4	0.2	0.1	0.1	0.1	0.1	0.1
Ni	0.19	0.01	0.00	0.00	0.01	0.01	0.01	0.01	0.01	0.01
Cu	0.15	0.01	0.01	0.01	0.02	0.02	0.02	0.01	0.01	0.01
No.	**11**	**12**	**13**	**14**	**15**	**16**	**17**	**18**	**19**	**20**
Depth, m	796	801	807	812.3	819.5	820	822.7	826.8	832	844.8
SiO_2	48.3	47.9	48.4	37.0	38.4	35.7	40.0	47.6	46.1	56.3
TiO_2	0.84	0.85	0.91	0.41	0.35	0.48	0.45	0.41	0.79	0.47
Al_2O_3	17.1	17.4	16.9	6.6	8.4	5.9	15.4	18.8	16.5	10.6
FeO tot.	8.9	10.4	10.2	14.1	13.9	14.3	11.4	8.8	13.0	4.1
MnO	0.14	0.16	0.16	0.19	0.20	0.19	0.11	0.13	0.17	0.10
MgO	9.6	8.4	8.0	27.1	24.1	28.0	12.5	8.3	7.5	4.3
CaO	11.4	11.0	11.2	4.9	6.1	4.4	8.1	12.1	10.6	16.5
Na_2O	1.8	1.9	2.0	0.4	0.5	0.5	1.0	1.8	2.0	2.9
K_2O	0.4	0.6	0.4	0.2	0.3	0.2	0.4	0.5	0.7	1.7
P_2O_5	0.12	0.11	0.16	0.05	0.06	0.06	0.07	0.05	0.10	0.08
Cr_2O_3	0.13	0.16	0.21	0.48	0.19	0.13	0.10	0.10	0.05	0.04
LOI	1.10	1.00	1.21	6.30	5.39	6.97	4.84	0.91	1.15	0.00
S	0.1	0.1	0.2	1.0	0.9	1.1	1.9	0.3	1.1	1.6
Ni	0.02	0.02	0.03	0.57	0.48	0.74	0.87	0.05	0.07	0.04
Cu	0.02	0.01	0.02	0.75	0.71	1.22	2.66	0.11	0.17	1.23
No.	**21**	**22**	**23**	**24**	**25**	**26**	**27**	**28**	**29**	**30**
Depth, m	65.2	75.8	80.2	LOD	BCR-2 *	BCR-2 **	DTS-2 *	DTS-2 **	BHVO-1 *	BHVO-1 **
SiO_2	46.2	45.0	48.6	0.04	53.8	54.1	39.8	39.4	49.6	49.9
TiO_2	1.77	0.99	0.87	0.005	2.31	2.26			2.46	2.37
Al_2O_3	15.7	15.4	15.4	0.020	13.8	13.5	0.42	0.45	13.7	13.5
FeO tot.	13.2	11.0	10.7	0.002	12.3	12.4	7.1	7.0	10.9	11.1
MnO	0.22	0.21	0.15	0.002	0.18	0.20	0.10	0.11	0.16	0.17
MgO	6.5	8.4	9.9	0.05	3.71	3.59	50.0	49.4	7.19	7.23
CaO	11.3	12.1	7.5	0.03	6.94	7.12	0.12	0.12	11.3	11.4
Na_2O	1.6	2.3	2.1	0.02	3.24	3.16			2.31	2.22
K_2O	0.6	1.1	2.1	0.007	1.71	1.79			0.54	0.52
P_2O_5	0.12	0.02	0.12	0.004	0.31	0.35			0.29	0.27
Cr_2O_3	0.02	0.06	0.01	0.005			0.22	0.23	0.04	0.04
LOI	2.11	2.48	2.63	0.005						
S	0.6	0.3	0.7	0.02						
Ni	0.11	0.01	0.21	0.0005			0.39	0.38	0.011	0.012
Cu	0.13	0.01	0.22	0.0006					0.013	0.013

Note. No. 1–20—borehole SF-10, 21–23—borehole EM-6. LOD—detected limit. *—USGS mesuared, **—USGS certified. LOI— Loss on ignition.

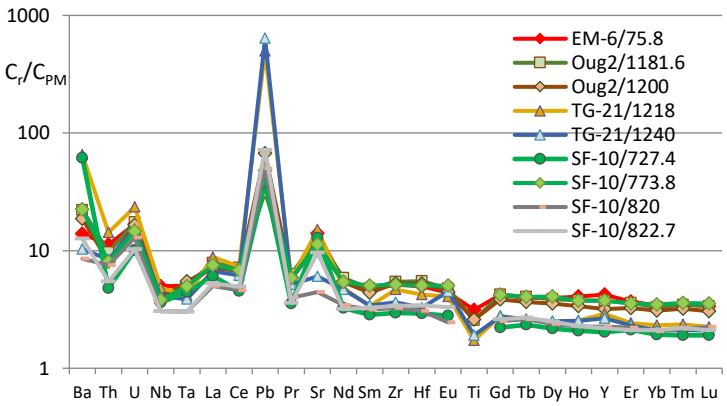

Figure 6. Spider-diagrams for rocks of the Talnakh intrusion Normalized to Primitive Mantle (PM). Data in Table 2. Branches: boreholes OUG-2, SF-10—North-Eastern, EM-6—South-Western, TG-21—South-Western.

Table 2. Rare elements in rocks of the Talnakh intrusion, ppm.

No.	1	2	3	4	5	6	7	8	9	10	11	12
N sample	1181.6	1200	1218	1240	727.4	773.8	820	822.7	75.8	LOD	BHVO-2 *	BHVO-2 **
Be	0.42	0.42	0.68	0.58	0.22	0.29	0.19	0.28	0.39	0.05	0.91	1.08
Sc	26	23	16	15	17	33	17	12	43	0.02	31.6	31.8
V	182	178	90	104	182	210	130	117	187	0.02	327	318
Cr	380	938	180	171	4740	464	367	248	780	0.18	287	287
Co	47	52	41	27	83	37	174	170	51	0.01	45.0	44.9
Ni	254	287	539	229	1870	112	4660	6000	210	0.16	121	120
Cu	134	91	893	708	1330	73	5330	9000	81	0.45	130	129
Zn	61	68	281	470	79	84	85	117	64	0.14	103	104
Rb	15	3.4	87	17	72	15	6.2	18	25	0.29	9.28	9.26
Sr	268	230	317	127	271	239	94	203	295	0.57	392	394
Y	17	15	13	12	9.2	17	10	9.9	19	0.003	24.7	25.9
Zr	61	59	52	41	33	57	36	38	58	0.14	171	171
Nb	2.8	2.8	3.5	2.9	2.6	2.7	2.2	2.2	3.5	0.15	18.0	18.1
Cs	0.74	0.47	0.96	0.29	1.9	0.71	0.23	1.3	0.49	0.14	0.10	0.10
Ba	154	130	456	72	430	156	60	89	97	0.33	0.13	131
La	5.4	4.9	6.1	4.6	4.2	5.2	3.4	3.6	5.0	0.01	15.2	15.2
Ce	13	12	13	11	8.0	12	8.2	8.8	12	0.01	37.5	37.5
Pr	1.7	1.6	1.6	1.4	0.98	1.6	1.1	0.99	1.6	0.001	5.27	5.34
Nd	7.9	7.3	6.5	6.3	4.4	7.3	4.7	4.3	7.5	0.004	24.0	24.3
Sm	2.1	1.9	1.5	1.5	1.3	2.2	1.4	1.5	2.1	0.005	6.07	6.02
Eu	0.80	0.75	0.69	0.76	0.47	0.84	0.41	0.56	0.74	0.002	2.03	2.04
Gd	2.5	2.3	1.7	1.6	1.3	2.5	1.5	1.6	2.5	0.005	6.00	6.21
Tb	0.44	0.39	0.28	0.28	0.25	0.44	0.28	0.29	0.43	0.01	0.96	0.94
Dy	2.8	2.6	1.8	1.9	1.6	3.0	1.8	1.8	2.9	0.005	5.24	5.28
Ho	0.62	0.55	0.42	0.41	0.34	0.61	0.37	0.37	0.67	0.003	0.97	0.99
Er	1.7	1.6	1.2	1.1	1.0	1.7	1.1	1.0	1.8	0.001	2.38	2.51
Tm	0.26	0.24	0.17	0.16	0.14	0.27	0.16	0.16	0.26	0.02	0.33	0.33
Yb	1.6	1.5	1.1	1.0	1.0	1.7	1.0	1.0	1.7	0.004	1.95	1.99
Lu	0.25	0.23	0.17	0.16	0.14	0.26	0.17	0.16	0.25	0.001	0.28	0.28
Hf	1.7	1.6	1.3	1.0	0.90	1.6	0.95	1.1	1.5	0.06	4.53	4.47
Ta	0.21	0.22	0.17	0.16	0.18	0.20	0.12	0.12	0.21	0.07	1.18	1.15
W	0.15	0.38	0.86	0.78	0.29	0.26	0.08	0.08	0.61	0.04	0.18	0.25
Tl	0.08	0.05	0.33	0.06	0.65	0.08	0.07	0.24	0.12	0.001	0.03	0.02
Pb	2.2	4.8	35	45	2.7	3.4	3.6	5.1	2.4	0.09	1.53	1.65
Bi	0.03	0.03	0.15	0.16	0.11	0.03	0.18	0.47	0.04	0.01	0.02	0.01
Th	0.82	0.69	1.2	0.71	0.41	0.69	0.64	0.46	0.95	0.03	1.28	1.22
U	0.37	0.35	0.50	0.32	0.21	0.31	0.27	0.22	0.35	0.001	0.412	0.41

Note. N sample—depth, m; No. 1–2—borehole OUG-2, 3–4—TG-21; 5–8—SF-10, 11—EM-6. 1–4—after [34]; major component for 5–9 in Table 1. LOD—detection limit, * standart, ** certified.

4.3. The Southern 2 Orebody

4.3.1. Morphology

The Southern 2 orebody is confined to the Southern part of the massif, where its upper part is eroded and covered by Quaternary sediments (Figure 3). The area of intrusive rocks reaching the surface is 3 km^2. It is difficult to judge the shape of the roof of an intrusive body, but the bottom strongly undulates. Complete sections of intrusive rocks occur only in the Northern part of this block where powerful magmatic breccias are widespread in the upper part. The horizons of contactic, taxitic and picritic gabbro-dolerites, as well as olivine gabbros are distinguished in this cross-section (from the bottom to top). Their thickness varies irregularly. In the Southern part of the intrusive body where the Southern 2 orebody is located, the following horizons were recognized (from top to botton): magmatic breccias, gabbro-diorites, gabbro-dolerites, olivine-bearing gabbro-dolerites, and taxitic gabbro-dolerites (Figure 7).

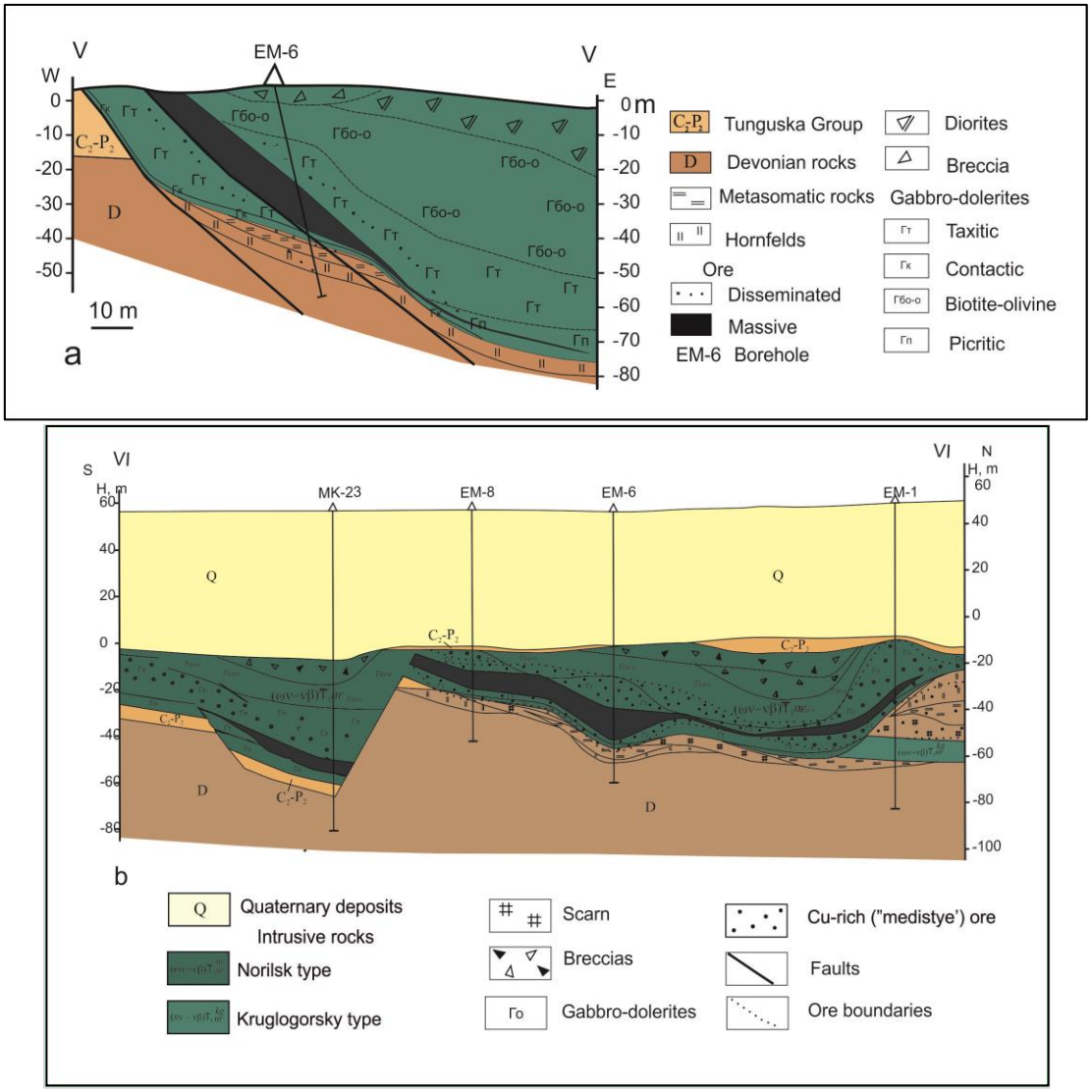

Figure 7. Position of the Southern 2 orebody inside the South-Westbranch, the cross-sections V-V (**a**) and VI-VI (**b**) (after Ltd. Norilskgeologia data with author's corrections).

The Southern 2 orebody takes an unusual position for massive ore. It is not confined to the bottom of the intrusion, but occurs in its Western flank. It has a steep inclinations (up to 45°) near the roof changing to 10° at the bottom (Figure 7). Its second specific feature is that it almost entirely lies in intrusive rocks (mostly in taxitic rocks). In general, it has a lenticular shape, with rare ramifications on individual branches. Its boundaries are clear, usually tectonic. Massive ores are surrounded by a halo of disseminated ores above and below it. The length of the Southern 2 orebody is 700 m, and the maximum thickness is 15 m.

4.3.2. Chemical Composition of the Ores

The predominance of chalcopyrite and bornite in ores reflects the high-copper composition of the Southern ore body. Copper concentrations vary from 19 to 25 wt % (Table 3), but nickel concentrations are also high (3–6 wt %) due to the large amount of pentlandite. The ratio of copper to nickel is 3.2–8.6 in the ore (in disseminated ores is 4.8–5.1). The cobalt content is extremely low, a few hundredths of a percent. S/Se varies in massive ore in a small range from 0.31 to 0.44; it is 0.44 in disseminated ore. These ratios are different from the Cu/Ni and S/Se ratios in ore from the North-Western branch (TG-21) and in the semi-massive ore of the Norilsk 2 intrusion (Samples N2/2, N2/4; N2/4a, Table 3, No. 23–25) where the first is equal to 1 and the second riches 1.89. The contents of theplatinum group elements are extremely high in all samples of massive ores, ΣPt + Pd + Rh reaches

280 ppm, and their content in the disseminated sulfides reaches 350 ppm (calculations in 100% sulfides). The distributions of PGE in disseminated and massive ore penetrated by borehole EM-6 is shown in Figure 8. PGE contents are high across whole body of the massive ore.

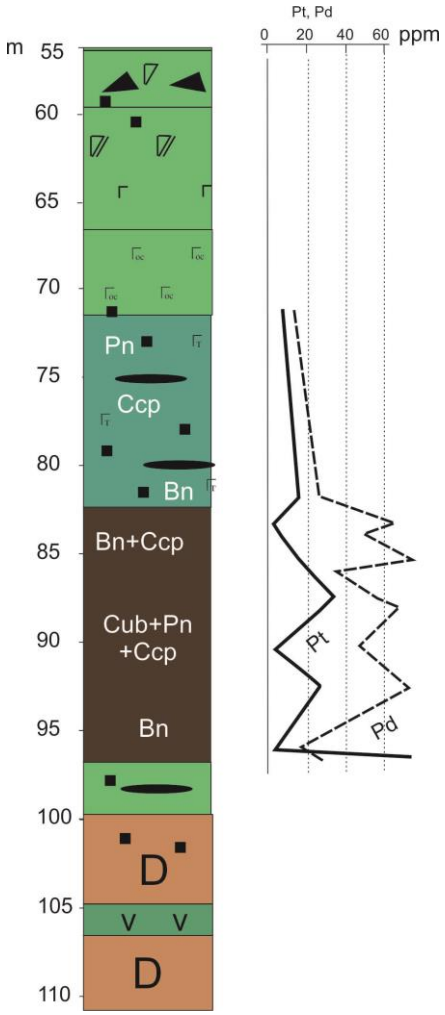

Figure 8. Structure of South-Western branch in borehole EM-6 and PGE distribution in ore. Data in Table 3.

Table 3. Chemical composition of sulfide ore.

No.	1	2	3	4	5	6	7	8	9
Sample	MA-12a	MA-13a	Ma-14a	MA-15a	MA-16a	MA-17a	EM-6/71.0	EM-6/81.0	EM-6/83.3
Cu	23.33	23.02	25.28	20.50	20.36	24.70	2.78	3.93	24.44
Ni	3.93	5.64	2.95	3.88	3.86	4.35	0.58	0.77	1.67
Co	0.06	0.10	0.05	0.06	0.06	0.07	0.017	0.01	0.02
Fe	22.96	22.42	23.08	25.88	27.93	23.78	15.32	16.70	25.82
S	50.20	48.30	51.50	50.30	49.30	49.40	3.19	4.53	47.20
As	0.94	1.51	1.50	2.75	1.20	2.56			1.09
Se	124	133	121	152	124	121	7.2	10.2	153
Ag	37.6	38.1	38.4	63.5	81.3	47.8	10.2	21.7	49.3
Au	0.9	1.26	2.67	10.1	0.4	8.3	0.85	2.44	1.16
Pt	2.6	1.5	9.6	124	2.5	5.4	3.31	8.86	0.9
Pd	36.5	48	47.5	155	115	97.5	10.6	22.6	66.5
Rh	1.32	1.24	0.95	1.28	0.92	0.88	0.12	0.38	0.78
Ir	0.09	0.09	0.10	0.10	0.10	0.09			0.10
Ru	0.09	0.08	0.06	0.08	0.07	0.06			0.05
Pb	215	211	220	297	248	253	12.80	16.20	237
Zn	61	50	61	609	586	56	7.80	8.32	696
Sn	8.51	7.78	12.85	58.76	14.42	13.72			8.56
Te	24.42	26.98	30.49	37.89	28.29	25.91			38.95

Mn	18.9	16	16.2	33.6	81.4	19.9			64
Mo	10.03	13.31	6.71	7.65	8.69	10.26			3.54
Sr	4.47	4.98	4.84	6.31	6.22	4.36			7.08
P	308	292	313	300	301	291			327
Ba	2.8	2.5	2.3	5.0	4.9	2.5			3.7
No	10	11	12	13	14	15	16	17	
Sample	EM-6/84.7	EM-6/85.5	EM-6/86.2	EM-6/87.8	EM-6/88.5	EM-6/90.8	EM-6/93	EM-6/95	
Cu	19.03	21.87	24.28	20.52	24.17	21.95	23.30	11.00	
Ni	4.83	3.84	3.30	5.36	3.72	3.16	4.92	3.44	
Co	0.08	0.06	0.05	0.09	0.06	0.05	0.08	0.09	
Fe	25.53	26.17	25.99	24.36	23.65	24.87	25.06	36.47	
S	50.00	49.00	45.80	45.20	48.40	49.20	45.80	51.30	
As	0.71	0.97		1.08	1.34	1.04	0.78	0.35	
Se	126	129	132	113	129	119	137	73	
Ag	58.2	35.4	72.2	51.4	39.7	52.6	70.3	10.56	
Au	0.37	1.51	0.28	1.33	6.98	0.85	2.35	0.21	
Pt	2.9	8.3	20.6	28.9	22	2.3	25.1	1.4	
Pd	43.7	75.85	32.5	58.3	70	45	75	14.5	
Rh	0.91	0.83	1.12	1.01	0.94	0.88	0.88	0.51	
Ir	0.09	0.11	0.10	0.10	0.09	0.09	0.10	0.10	
Ru	0.07	0.07	0.11	0.06	0.06	0.06	0.07	0.07	
No	10	11	12	13	14	15	16	17	
Pb	199	211	209	266	232	224	203	127	
Zn	558	590	470	470	568	543	550	103	
Sn	8.18	8.91	7.91	16.43	14.38	11.26	27.07	8.53	
Te	21.82	23.57	24.21	26.38	22.58	23.73	23.09	13.21	
Mn	143.6	37.9	55.8	41.8	48.6	38.55	15.9	11.67	
Mo	10.65	9.19	11.77	7.54	8.99	6.93	11.12	6.57	
Sr	13.58	8.62	8.54	16.96	8.78	11.26	5.22	3.81	
P	310	360	292	304	306	316	317	323	
Ba	3.1	3.5	3.2	3.3	5.4	4.3	3.2	2.3	
No	18	19	20	21	22	23	24	25	
Sample	EM-6/96.4	TG-21/1316.4	TG-21/1333.6	TG-21/1361.9	TG-21/1362	N2/4a	N2/2	N2/4	
Cu	20.04	0.01	0.59	1.74	2.25	1.75	0.87	2.18	
Ni	6.17	0.02	0.35	3.07	3.27	2.01	0.52	2.34	
Co	0.11	0.01	0.02	0.13	0.13	0.10	0.02	0.11	
Fe	24.68	7.43	12.61	34.16	31.40	30.05	10.78	36.17	
S	48.40	0.05	1.99	34.96	33.50	24.68	6.66	40.33	
As	0.42	3.41	3.12	1.91	1.48	0.60	3.34	0.32	
Se	82	6	10	19	56	45	21	21	
Ag	12.3	1.05	2.42	7.96	2.95	5.31	2.89	2.81	
Au	0.97	0.01	0.01	0.01	0.01	0.04	0.18	0.03	
Pt	78	1.93	0.31	1.64	0.35	0.19	2.52	0.07	
Pd	27.7	0.06	2.40	0.67	4.06	4.21	5.85	4.45	
Rh	1.02		0.15		3.50	3.35	1.31	3.10	
Ir	0.16								
Ru	0.11								
Pb	209	17	34	23	17	26	34	13	
Zn	59	66	590	45	32	66	47	61	
Sn	12.66								
Te	3.71	0.03	0.09	0.34	0.44	1.29	1.08	2.36	
Mn	42.3	970	1400	290	510	670	720	790	
Mo	13.81								
Sr	5.02	248.00	156.00	61.30	88.20	162.00	254.00	143.00	
P	302	560	380	490	660	660	480	540	
Ba	2.9	128.4	63.2	19.1	24.9	27.7	130.4	13.1	

Note. Cu, Ni, Co., Fe, S—in wt %, other elements—in ppm. No. 1–18—the South-Western branch; 19–22—North-Western branch, TG-21; 23–25—massive ore, Norilsk 2. Sample N (analyses 7–20) = name borehole/depth, m. Empty cell—element was not analyzed.

4.3.3. Mineral Composition of the Ores

A distinctive feature of the ore assemblage of the Southern 2 orebody is the large predominance of chalcopyrite over other sulfides in comparison with the ores from the other branches, where

pyrrhotite predominates (Figure 9). The pentlandite-cubanite-chalcopyrite assemblage is the main type of ores (Figure 10a–d) whereas the chalcopyrite-pyrrhotite type is rare. An unusual feature of these ores is the widespread bornite in massive and disseminated ores which occurs both over massive ores (endocontact) and under the orebody into exocontact (Figure 10e–h).

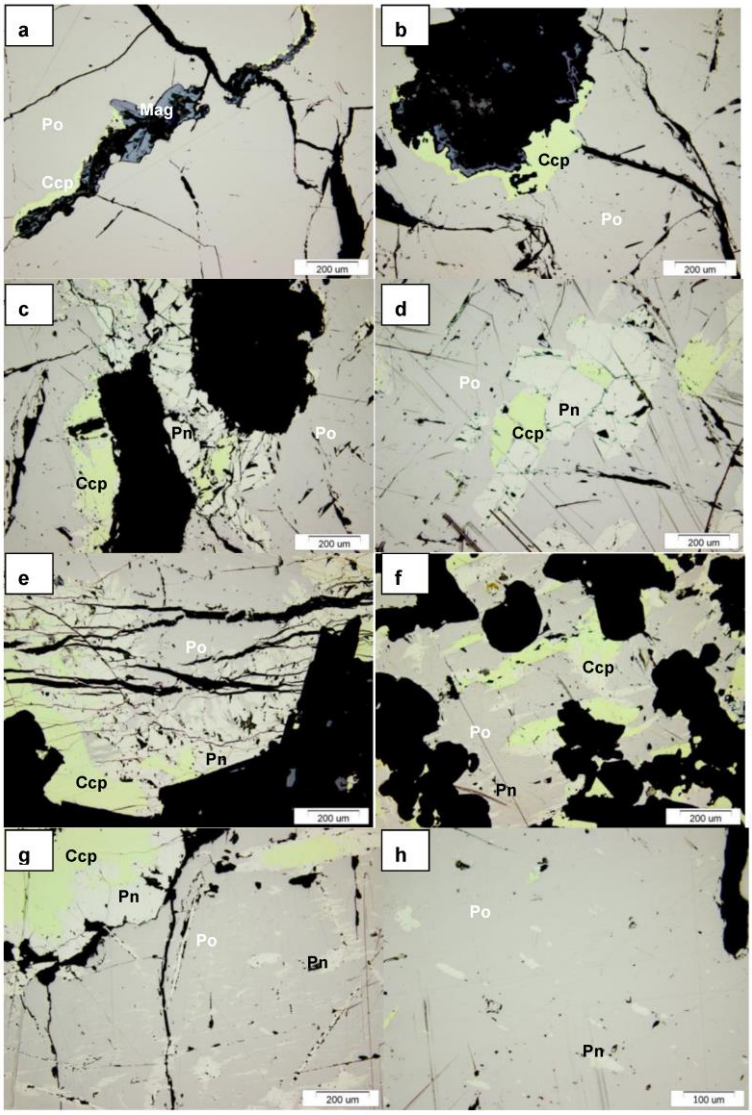

Figure 9. Photomicrographs of the ore from North-Eastern branch of the Talnakh intrusiona-f—borehole SF-10, depth, m: (**a**,**b**)—726; (**c**,**d**)—817; (**e**,**f**)—818; (**g**,**h**)—borehole OUG-2, depth 1211 m. Here and in Figure 12: Po—pyrrhotite, Pn—pentlandite, Ccp—Chalcopyrite, Mag—magnetite.

Chalcopyrite is represented only by tetragonal species (Tables 4 and 5), while the other minerals of the chalcopyrite group (talnakhite, moihkukite, putoranite) that are typical of the Oktyabr'skoe deposit were not found in the Southern 2 orebody. Cubanite is common in these ores similarly to the intermediate zone of the main orebody of the Kharaelakh intrusion, but an abundance of pentlandite in the Southern 2 distinguishes them from it. Pentlandite occurs as two morphological varieties (Figure 10b,d): (i) large euhedral crystals, due to ores sometimes acquiring the porphyry structure; and (ii) flame-like grains in chalcopyrite, cubanite, and pyrrhotite. The first morphological variety is more common. Crystals of pentlandite up to 1 cm in size are fractured and the cracks are filled with violarite replacing chalcopyrite. The composition of Southern 2 pentlandite differs from other deposits in the Norilsk region [19,24,43] by the lower concentrations of cobalt (0.38–0.73 wt % Co versus 1–2 wt %, respectively), as well as by the prevalence of Ni-rich pentlandite (Fe/Ni < 1). A characteristic feature of pentlandite from the Southern 2 orebody is frequent Cu in its composition

(up to 3.4 wt %, Table 4). Inclusions of sphalerite, galena and veins of magnetite are found often in chalcopyrite. Magnetite occur sometimes as myrmecitic aggregates with chalcoprite. Minor copper amount there is in all ore minerals of the orebody: millerite (1–4.4 wt %), pyrite (0.18 wt %), pyrrhotite (0.11–0.12 wt %). Idaite, pyrite and MSS are rare minerals in the studied ores (Table 5).

A specific feature of the Southern 2 orebody is the presence of a large amount of chalcocite-bornite and chalcopyrite-bornite mineralogical varieties in the endo- and exo-contacts of the intrusion: both in gabbro and in the sandstones underlying the intrusion (and in the hornfels developed on them). Sometimes only one bornite occurs in the orebody (Figure 10). Furthermore, small clusters of chalcopyrite (10–12 cm) surrounded by a border of bornite have been found in the upper part of the Southern 2 orebody. Chalcopyrite and bornite are in form of veins in disseminated ore, while the chalcocite is in the interstitium of rock-forming minerals as a rule (Figure 10g,h).

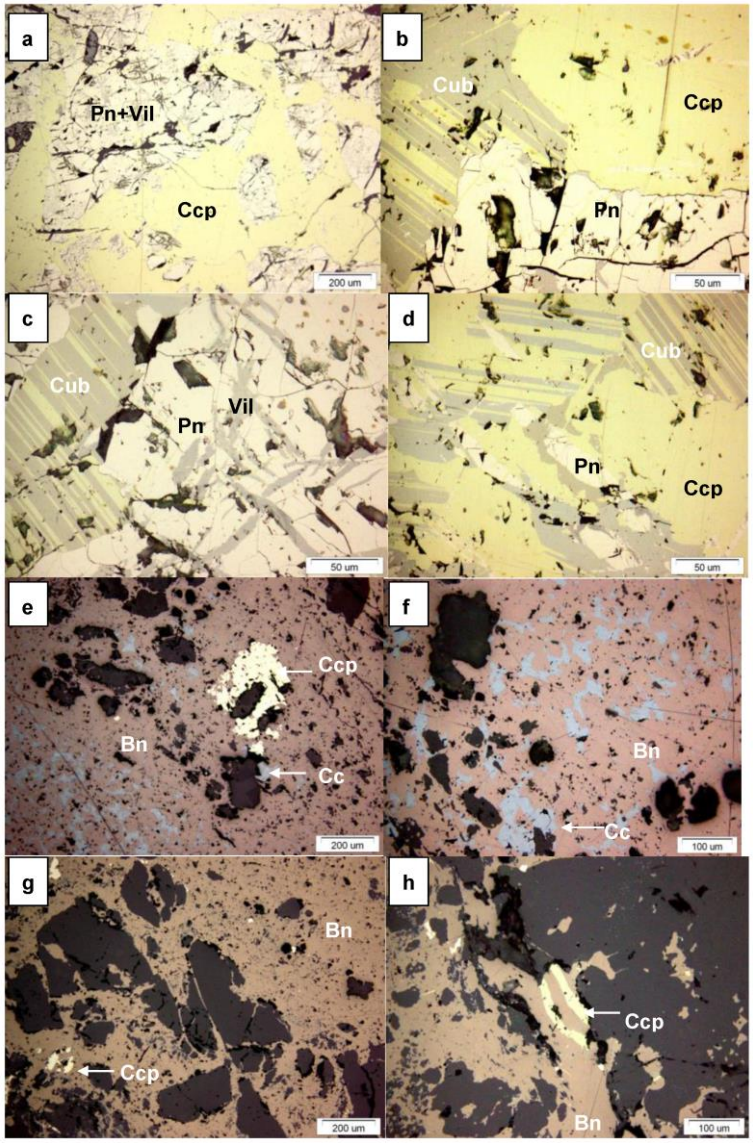

Figure 10. Photomicrographs of the ore from South-Western branch of the Talnakh intrusion. Borehole EM-6: (**a**–**f**)—massive ore, (**g**,**h**)—disseminate ore. Minerals: Bn—bornite, Cc—chalcocite, Vil—violarite, Cub—cubanite.

Table 4. Minerals of the Southern 2 orebody.

Main	Major	Rare (PGM)
Chalcopyrite $CuFeS_2$	Bornite Cu_5FeS_4	Majakite PdNiAs
Pentlandite $(Ni,Fe,Co)_9S_8$	Chalcocite Cu_2S	Palladoarsenide Pd_2As
Cubanite $CuFe_2S_3$	Pyrite FeS_2	Stillwaterite $(Pd,Ni)_8As_3$
		Zvyagintsevite Pd_3Pb Plumbopalladinite Pd_3Pb_2 Polarite Pd(Pb,Bi)
Pyrrhotite $Fe_{1-x}S$	Magnetite $FeFe_2O_4$ Violarite $FeNi_2S_4$ Sphalerite ZnS Galena PbS	Rustenburgite $(Pt,Pd)_3Sn$ Atokite $(Pd,Pt)_3Sn$ Taimyrite $(Pd,Cu,Pt)_3Sn$ Stannopalladinite Pd_5Sn_2Cu Auricupride $Cu_3(Au,Pd)$ Tetra-auricupride Cu(Au,Pd) Cu-Au-Ag alloys Guanglinite Pd_3As Sobolevskite PdBi

Table 5. Composition of ore minerals from the Southern 2 orebody, wt %.

No.	Cu	Co	Ni	Fe	S	Total	Mineral
1	35.32	0.09	0.00	30.99	35.30	101.70	Chalcopyrite
2	34.52	0.10	0.01	31.10	34.95	100.68	Chalcopyrite
3	35.08	0.00	0.05	31.35	35.33	101.81	Chalcopyrite
4	34.35	0.00	0.04	31.01	35.05	100.45	Chalcopyrite
5	0.10	0.37	33.97	32.13	33.87	100.44	Pentlandite
6	1.44	0.52	31.33	31.27	35.00	99.56	Pentlandite
7	0.09	0.50	33.58	32.54	34.14	100.85	Pentlandite
8	0.72	0.47	33.98	32.10	33.49	100.76	Pentlandite
9	0.05	0.49	34.24	32.48	33.41	100.67	Pentlandite
10	0.75	0.66	32.29	29.91	34.80	98.41	Pentlandite
11	0.14	0.42	34.92	31.44	34.00	100.92	Pentlandite
12	0.30	0.63	34.70	30.86	33.65	100.14	Pentlandite
13	0.05	0.47	35.26	31.12	33.80	100.70	Pentlandite
14	0.05	0.45	33.91	30.23	34.48	99.12	Pentlandite
15	0.38	0.73	39.71	26.23	33.73	100.78	Pentlandite
16	1.34	0.19	27.67	36.71	33.63	99.54	Pentlandite
17	3.09	0.38	29.06	33.00	34.39	99.92	Pentlandite
18	3.42	0.43	36.07	26.85	33.51	100.28	Pentlandite
19	0.11	0.26	3.99	56.19	39.08	99.63	Pyrrhotite
20	0.12	0.47	7.53	55.56	36.91	100.59	Pyrrhotite
21	23.46	0.05	0.34	41.85	35.73	101.43	Cubanite
22	23.41	0.01	0.01	41.71	35.45	100.59	Cubanite
23	23.24	0.00	0.14	41.92	35.24	100.54	Cubanite
24	24.34	0.08	0.06	42.00	35.71	102.19	Cubanite
25	22.72	0.06	0.08	41.64	35.20	99.70	Cubanite
26	23.82	0.04	0.03	41.51	35.33	100.73	Cubanite
27	0.73	1.94	60.22	0.03	35.16	98.08	Millerite
28	1.01	1.43	60.91	0.03	35.49	98.87	Millerite
29	1.37	0.29	61.37	0.03	35.37	98.43	Millerite
30	1.55	0.27	62.04	0.09	35.17	99.12	Millerite
31	4.47	0.84	57.73	1.51	35.00	99.55	Millerite
32	79.18	0.07	0.00	0.56	21.54	101.35	Chalcocite
33	79.06	0.03	0.00	0.12	21.49	100.70	Chalcocite
34	79.59	0.00	0.00	0.06	21.07	100.72	Chalcocite
35	79.61	0.00	0.00	0.58	21.00	101.19	Chalcocite
36	60.23	0.01	0.08	13.74	25.32	99.38	Bornite
37	61.25	0.00	0.18	11.56	25.98	98.97	Bornite
38	63.22	0.00	0.00	11.05	25.56	99.83	Bornite
39	49.05	0.09	0.16	20.13	29.63	99.06	Idaite
40	8.98	0.44	26.22	30.01	34.44	100.09	mss
41	19.85	0.11	14.18	30.71	34.85	99.70	mss

4.3.4. Minerals of Platinum Group Elements (PGM)

Among the minerals of elements of the platinum group (PGE) in the Southen 2 orebody, the palladium minerals of the Pd-Cu-Sn system are predominant (37%) (Figure 11). Minerals of the systems Pd-Pb-Bi, Pd-Ni-As, Au-Ag-Pd-Cu and intermetallics of the Pt-Fe-Cu-Ni are also common (Table 4). In the Southern 2 orebody 12 PGMs were found: tetraferroplatinum Pt(Fe,Cu,Ni), majakite PdNiAs, palladoarsenide Pd_2As, guanglinite(?) Pd_3As, stillwaterite Pd_8As_3, polarite Pd(Pb,Bi), zvyagintsevite Pd_3Pb, plumbopalladinite Pd_3Pb_2, rustenburgite $(Pt,Pd)_3Sn$, atokite $(Pd,Pt)_3Sn$, stannopalladinite Pd_5Sn_2Cu, sobolevskite PdBi, as well as various unnamed phases: Pd_5Pb_3, $(Pd,Ni)_5As_2$, $(Ni,Pd)_5As_2$, $(Pd,Cu)_3(As,Sb,Sn)$ and Pd_3Bi_2.

Among the Pd minerals, stannopalladinite Pd_5Sn_2Cu predominates. It occurs in intergrowth with various PGMs: polarite, tetraferroplatinum, zvyagintsevite and unnamed phases.

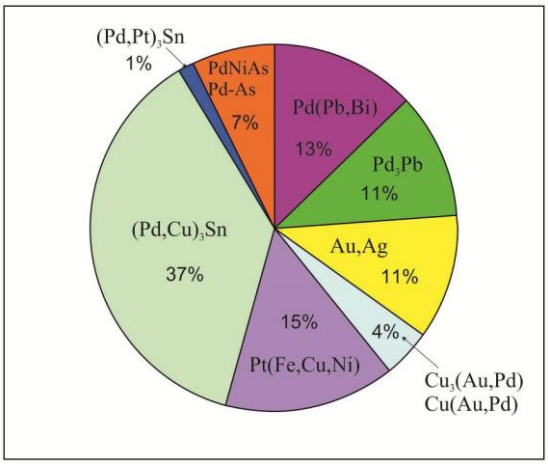

Figure 11. Relationships of the PGE minerals in ores of the Southern 2 orebody.

It differs from the mineral previously described in the literature by the excess of Cu in the composition of most of the grains, the amount of which above the one unit is added to Pd in the mineral formula: $(Pd,Cu)_5Sn_2Cu$. Rustenburgite and atokite are found in intergrowth together with a clear phase boundary between them (Figure 12a), although both these minerals form an extended series of solid solutions. Both these minerals contain Cu and Ni (Table 6).

Table 6. Mineral compositions in the system Pd-Pt-Cu-Sn from the Southern 2 orebody, wt %.

No.	Ni	Cu	Pt	Pd	Sn	Pb	Bi	Sb	As
1		7.62	1.32	62.17	21.41	1.02	0.76	5.82	
2		7.39	1.28	64.21	21.08	1.49	0.65	5.64	
3		7.77	1.16	63.83	21.79	0.78		4.7	
4		6.6	0.86	60.6	12.36	18.48		2.07	
5		6.74	0.96	60.15	14.27	17.03		1.26	
6		9.15	1.33	61.44	22.23	1.54		4.03	
7		8.75	1.41	61.59	21.86	1.62		4.71	
8		8.41	0.9	62.98	25.04	0.97		2.33	
9		8.94	1.54	60.9	23.16	2.73	0.54	2.44	
10		9.19	3.75	59.97	26.13				
11		9.42	1.9	61.32	25.62	1.72			
12		9.53	3.39	59.46	25.94	1.05		1.32	0.28
13		8.59	2.08	58.07	19.98	9.83		0.65	0.26
14		9.28	2.35	58.53	20.79	8.86		1.04	
15		8.68	1.31	58.46	16.99	13.68		0.87	
16	1.65	1.13	63.09	14.59	17.92				
17	1.92	2.03	62.99	14.05	17.92				
18	0.36	9.25	26.15	39.56	22.85				
19	0.27	1.53	30.87	44.25	22.05				

Note. 1–15—stannopalladinite Pd_5Sn_2Cu; 16–17—rustenburgite $(Pt,Pd)_3Sn$; 18–19—atokite $(Pd,Pt)_3Sn$.
1: $(Pd_{4.93}Pt_{0.06})_{4.99}(Sn_{1.52}Sb_{0.40}Pb_{0.04}Bi_{0.03})_{1.99}Cu_{1.01}$;

2: $(Pd_{5.03}Pt_{0.05})_{5.08}(Sn_{1.48}Sb_{0.39}Pb_{0.06}Bi_{0.03})_{1.96}Cu_{0.97}$; 3: $(Pd_{5.03}Pt_{0.05})_{5.08}(Sn_{1.54}Sb_{0.32}Pb_{0.03})_{1.89}Cu_{1.03}$;
4: $(Pd_{5.13}Pt_{0.04})_{5.17}(Sn_{0.94}Pb_{0.80}Sb_{0.15})_{1.89}Cu_{0.94}$; 5: $(Pd_{5.09}Pt_{0.04})_{5.13}(Sn_{1.08}Pb_{0.74}Sb_{0.09})_{1.91}Cu_{0.95}$;
6: $(Pd_{4.83}Pt_{0.06})_{4.89}(Sn_{1.57}Sb_{0.28}Pb_{0.06})_{1.91}Cu_{1.20}$; 7: $(Pd_{4.85}Pt_{0.06})_{4.91}(Sn_{1.54}Sb_{0.32}Pb_{0.07})_{1.93}Cu_{1.15}$;
8: $(Pd_{4.91}Pt_{0.04})_{4.95}(Sn_{1.75}Sb_{0.16}Pb_{0.04})_{1.95}Cu_{1.10}$; 9: $(Pd_{4.81}Pt_{0.07})_{4.88}(Sn_{1.64}Sb_{0.17}Pb_{0.11}Bi_{0.02})_{1.94}Cu_{1.18}$;
10: $(Pd_{4.76}Pt_{0.16})_{4.92}Sn_{1.86}Cu_{1.22}$; 11: $(Pd_{4.81}Pt_{0.08})_{4.89}(Sn_{1.80}Pb_{0.07})_{1.87}Cu_{1.24}$;
12: $(Pd_{4.64}Pt_{0.14})_{4.78}(Sn_{1.81}Sb_{0.09}Pb_{0.04}As_{0.03})_{1.97}Cu_{1.24}$; 13: $(Pd_{4.77}Pt_{0.09})_{4.86}(Sn_{1.47}Pb_{0.41}Sb_{0.05}As_{0.03})_{1.96}Cu_{1.18}$;
14: $(Pd_{4.71}Pt_{0.10})_{4.81}(Sn_{1.50}Pb_{0.37}Sb_{0.07})_{1.94}Cu_{1.25}$; 15: $(Pd_{4.84}Pt_{0.06})_{4.95}(Sn_{1.26}Pb_{0.58}Sb_{0.06})_{1.90}Cu_{1.20}$;
16: $(Pt_{1.97}Pd_{0.83}Ni_{0.17}Cu_{0.11})_{3.08}Sn_{0.92}$; 17: $(Pt_{1.93}Pd_{0.79}Ni_{0.20}Cu_{0.19})_{3.11}Sn_{0.90}$; 18: $(Pd_{1.75}Cu_{0.68}Pt_{0.63}Ni_{0.03})_{3.09}Sn_{0.91}$;
19: $(Pd_{2.11}Pt_{0.80}Cu_{0.12}Ni_{0.02})_{3.05}Sn_{0.94}$.

A significant proportion (24%) of the mineral associations is represented by Pd-Pb(Bi) compounds (polarite, zvyagintsevite and unnamed phases of this system) (Table 7). Pb-containing minerals are in intergrowths with the other minerals of PGE (Figure 12b–d). In this case, the decomposition structure of the solid solutions between zvyaginsevite and Pd_5Pb_3 is often observed (Figure 12d). Between polarite Pb-rich composition are dominated: $Pd_{1.03}(Pb_{0.82}Bi_{0.15})_{0.97}$, although PdBi with a minor Pb as well as the $Pd_3(Bi,Pb)_2$ alsooccur in this association (Table 7). The unnamed phase Pd_5Pb_3 is widespread in this system. It contains a minor Ag (Table 7) unlike the other Pd-Pb minerals. In this case the compositions of this phase deviate from stoichiometry to the side of zvyagintsevite (Figure 13). Galena is found in intergrowths with Pb-bearing minerals.

Table 7. Mineral compositions in system Pd-Pb-Bi in the Southern 2 orebody, wt %.

No	Ag	Pd	Pb	Bi	Total	Formula
1		60.48	38.69		99.17	$Pd_{3.01}Pb_{0.99}$
2		61.45	38.95		100.4	$Pd_{3.02}Pb_{0.98}$
3		61.69	38.56		100.25	$Pd_{3.03}Pb_{0.97}$
4		61.57	38.18		99.75	$Pd_{3.03}Pb_{0.97}$
5		45.34	51.9		97.24	$Pd_{5.04}Pb_{2.96}$
6	3.44	43.12	51.11		97.67	$(Pd_{2.96}Ag_{0.23})_{3.19}Pb_{1.80}$
7	3.09	45.28	52.85		101.22	$(Pd_{3.00}Ag_{0.20})_{3.20}Pb_{1.80}$
8	3.37	44.75	52.44		100.56	$(Pd_{2.98}Ag_{0.22})_{3.20}Pb_{1.80}$
9	3.27	44.93	52.44		100.64	$(Pd_{2.99}Ag_{0.21})_{3.20}Pb_{1.79}$
10		35.38	54.86	9.75	99.99	$Pd_{1.03}(Pb_{0.82}Bi_{0.15})_{0.97}$
11		35.06	53.99	11.28	100.33	$Pd_{1.02}(Pb_{0.81}Bi_{0.17})_{0.98}$
12		35.31	49.83	14.72	99.86	$Pd_{1.03}(Pb_{0.75}Bi_{0.22})_{0.97}$
13		35.71	47.69	16.25	99.65	$Pd_{1.04}(Pb_{0.72}Bi_{0.24})_{0.96}$
14		34.47	43.53	21.57	99.57	$Pd_{1.02}(Pb_{0.66}Bi_{0.32})_{0.98}$
15		35	41.15	24.33	100.48	$Pd_{1.02}(Pb_{0.62}Bi_{0.36})_{0.98}$
16		35.55	35.78	27.64	98.97	$Pd_{1.05}(Pb_{0.54}Bi_{0.41})_{0.95}$
17		35.31	5.82	58.6	99.73	$Pd_{1.04}(Bi_{0.88}Pb_{0.09})_{0.97}$
18		35.89	4.08	60.76	100.73	$Pd_{1.04}(Bi_{0.90}Pb_{0.06})_{0.96}$
19		38.9	4.38	46.46	89.74	$Pd_{3.00}(Bi_{1.83}Pb_{0.17})_{2.00}$

Note. 1–4—zvyagintsevite Pd_3Pb; 5–9—unnamed phase Pd_5Pb_3; 10–16—polarite Pd(Pb,Bi); 17–18—polarite Pd(Bi,Pb); 19—unnamed phase $Pd_3(Bi,Pb)_2$.

Pt-Fe-Cu-Ni alloys in the chalcopyrite ores of the Southern 2 orebody occur in association with stannopalladinite (Figures 12b,d). They are the latest phases in ores compared with other PGE minerals. These alloys have the same composition in the different grains (Table 8) and the points of their compositions lie in the tetraferroplatinum field on the diagram Pt-Fe-Ni (Figure 13), although they contain about 10 mol % of the tulameenite and about 15 mol % of ferronickelplatinum. Tetraferroplatinum contains Pd and Rh as minor elements (Table 8).

Table 8. Composition of tetraferroplatinum in the Southern 2 orebody, wt %.

No.	Pt	Pd	Ni	Cu	Fe	Rh	Total
1	76.65	0.14	3.45	2.79	15.08	0.06	98.17
2	75.71	0.19	3.65	2.5	15.2		97.25
3	76.13	0.41	4	2.38	15.77	0.06	98.75
4	75.47	0.28	3.74	2.38	15.84	0.11	97.81

5	75.86	0.27	3.56	2.84	16.02		98.55
6	77.52	0.29	3.79	2.5	16.02	0.05	100.17
7	76.41	0.26	3.76	2.51	16.16	0.09	99.19
8	75.39	0.35	3.67	2.42	16.18	0.13	98.13
9	76.27	0.17	3.77	2.55	16.33	0.13	99.22
10	76.08	0.28	3.63	2.66	16.45	0.26	99.36

Minerals of the Pd-Ni-As system are 7% of the total amount of PGM. Palladoarsenide, guanglinite, stillwaterite, majakite have also been found (Table 9). They occur as euhedral crystals (Figures 12c and 14). The main feature of these minerals is the significant Ni concentrations in the Pd-As minerals, close to their nickel analogs in Pd-Ni-As system (Table 9). The unidentified phase $(Pd,Cu)_3(As,Sb,Sn)$, possibly is guanglinite (Pd_3As) which is considerably enriched by other elements.

Tetra-auricupride Cu(Au,Pd) predominates among the minerals of the Au-Pd-Ag-Cu system while auricupride $Cu_3(Au,Pd)$, electrum and Ag-rich alloys are much less common (Table 10). They form intergrowths with other PGM taking the intersticial position between them. In this case, tetraauricupride is a precursor mineral in comparison withAu-Ag alloys (Figure 12c,e).

Table 9. Mineral compositions in the system Pd-Ni-As of the Southern 2 orebody, wt %.

No.	Pd	Ni	Cu	Fe	Co	As	Sb	Sn	Pb	Total
1	45.24	23.53				30.37				99.14
2	46.22	24.15				31.08				101.45
3	45.44	22.95			0.09	30.08				98.56
4	45.01	23.43			0.11	29.53				98.08
5	45.22	23.67		0.05	0.11	29.63				98.68
6	68.12	4.57		0.07	0.14	25.55				98.46
7	52.73	14.65	0.25	0.54	0.11	30.37				98.65
8	81.02					20.15				99.31
9	80.57					20.42				99.39
10	80.48					20.96				101.44
11	77.33	0.8		0.11		20.78				99.02
12	28.98	42.78				27.56				99.32
13	64.96	10.01		0.09	0.14	24.36				99.56
14	29.29	39.33	0.34			28.44				97.6
15 *	68.37	0.93	5.3			9.86	9.39	6.24	0.46	100.55
16 *	68.61	1.04	5.31			9.9	9.6	6	0.62	101.08
17 *	67.48	0.67	6.1			10	6.59	7.23	2.26	100.33

Note. 1–5—majakite PdNiAs, 6–7—palladoarsenide Pd_2As, 8–9—guanglinite Pd_3As, 10–11—stillwaterite Pd_8As_3, 12—Ni—stillwaterite; 13–14— solid solutions $(Pd,Ni)_5As_2$; 15–17—unnamed phase $(Pd,Cu)_3(As,Sb,Sn)$. Formula: 1: $Pd_{1.04}Ni_{0.98}As_{0.99}$; 2: $Pd_{1.03}Ni_{0.98}As_{0.99}$; 3: $Pd_{1.05}Ni_{0.96}As_{0.99}$; 4: $Pd_{1.04}Ni_{0.98}As_{0.97}$; 5: $Pd_{1.04}Ni_{0.99}As_{0.97}$; 6: $(Pd_{1.81}Ni_{0.22}Co_{0.01})_{2.04}As_{0.96}$; 7: $(Pd_{1.27}Ni_{0.64}Fe_{0.02}Cu_{0.01})_{1.94}As_{1.04}$; 8: $Pd_{2.96}As_{1.04}$; 9: $Pd_{2.94}As_{1.06}$; 10: $Pd_{8.03}As_{2.97}$; 11: $(Pd_{7.83}Ni_{0.15}Fe_{0.03})_{8.01}As_{2.99}$; 12: $(Ni_{5.86}Pd_{2.19})_{8.05}As_{2.96}$; 13: $(Pd_{3.85}Ni_{1.08}Fe_{0.01}Co_{0.01})_{4.95}As_{2.05}$; 14: $(Ni_{3.52}Pd_{1.45}Cu_{0.03}Pt_{0.01})_{5.01}As_{2.00}$; 15: $(Pd_{2.56}Cu_{0.33}Ni_{0.06})_{2.95}(As_{0.52}Sb_{0.31}Sn_{0.22})_{1.05}$; 16: $(Pd_{2.55}Cu_{0.33}Ni_{0.07})_{2.95}(As_{0.52}Sb_{0.31}Sn_{0.22})_{1.05}$; 17: $(Pd_{2.53}Cu_{0.38}Ni_{0.05})_{2.96}(As_{0.53}Sb_{0.22}Sn_{0.24}Pb_{0.04})_{1.04}$.

Table 10. Mineral compositions in the system Au-Ag-Pd-Cu in the Southern 2 orebody, wt %.

No.	Cu	Au	Ag	Pd	Total	Formula
1	0.73	4.36	94.47		99.56	$Ag_{96.30}Au_{2.43}Cu_{1.26}$
2		13.87	89.61		103.48	$Ag_{92.19}Au_{7.81}$
3		16.18	84.46		100.64	$Ag_{90.50}Au_{9.50}$
4		17.41	81.25		98.66	$Ag_{89.50}Au_{10.50}$
5		17.55	79.98		97.53	$Ag_{89.27}Au_{10.73}$
6		18.2	82.5		100.7	$Ag_{89.22}Au_{10.78}$
7	0.79	18.24	80.09		99.12	$Ag_{87.61}Au_{10.93}Cu_{1.47}$
8		18.49	80.64		99.13	$Ag_{88.84}Au_{11.16}$

9		19.8	78.44		98.24	$Ag_{87.86}Au_{12.14}$
10	0.73	21.13	78.21		100.07	$Ag_{85.93}Au_{12.71}Cu_{1.36}$
11		21.95	77.8		99.75	$Ag_{86.62}Au_{13.38}$
12		22.14	76.77		98.91	$Ag_{86.36}Au_{13.64}$
13		23.04	74.67		97.71	$Ag_{85.54}Au_{14.46}$
14		23.51	75.87		99.38	$Ag_{85.49}Au_{14.51}$
15	0.59	24.37	75.9		100.86	$Ag_{84.10}Au_{14.79}Cu_{1.11}$
16		26.18	71.71		97.89	$Ag_{83.34}Au_{16.66}$
17		30.55	68.28		98.83	$Ag_{80.32}Au_{19.68}$
18	0.58	86.75	4.69	5.28	97.3	$Au_{0.81}Pd_{0.09}Ag_{0.08}Cu_{0.02}$
19	0.29	72.91	22.42	2.63	98.25	$Au_{0.61}Ag_{0.34}Pd_{0.04}Cu_{0.02}$
20	47.19	42.42	0.21	7.68	97.5	$Cu_{2.87}(Au_{0.83}Pd_{0.29}Ag_{0.01})_{1.13}$
21	25.24	64.31	0.08	7.97	97.6	$(Au_{0.84}Pd_{0.16})_{1.00}Cu_{1.00}$
22	24.98	64	0.11	8.24	97.33	$(Au_{0.84}Pd_{0.17})_{1.01}Cu_{0.98}$

Note. 1–17—kustelite, 18–19—electrum, 20—auricupride $Cu_3(Au,Pd)$, 21–22—tetra-auricupride Cu(Au,Pd).

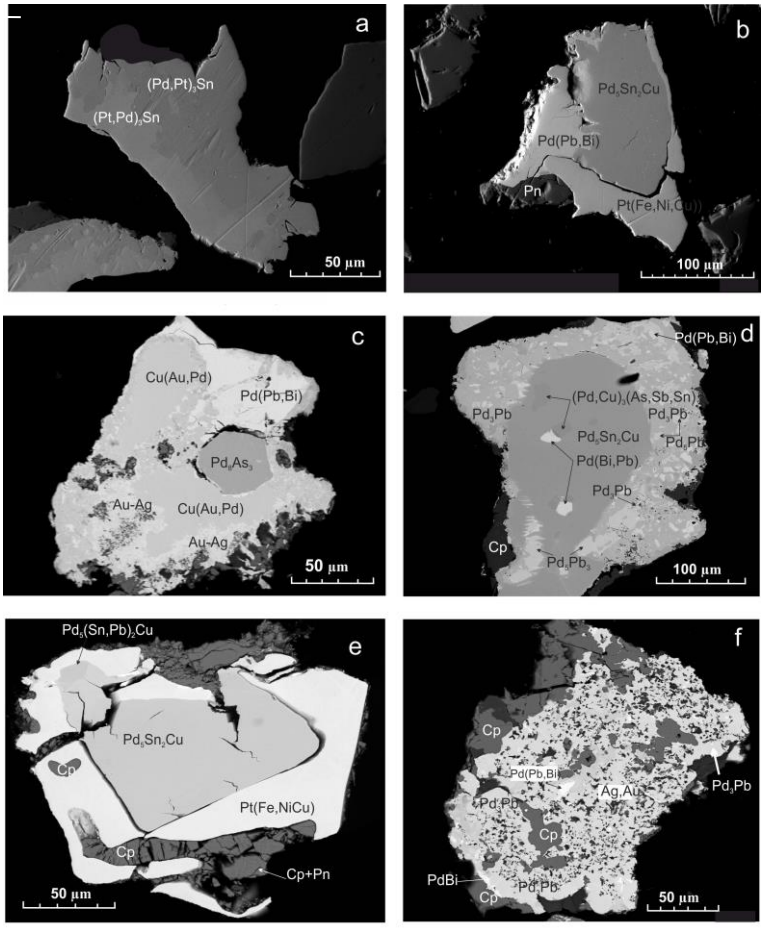

Figure 12. Back-scattered electrons images of the platinum group minerals in ore of the Southern 2 orebody. Data in Tables 6–10. (**a**)—intergrowth of atokite $(Pd,Pt)_3Sn$ and rustenburgite $(Pt,Pd)_3Sn$; (**b**)—intergrowth of polarite Pd(Pb,Bi) and stannopalladinite Pd_5Sn_2Cu in the frame of tetraferroplatinum Pt(Fe,Ni,Cu); (**c**)—euchedral inclusion of stillwaterite Pd_8As_3 in a aggregate consisting of polarite, tetra-auricupride Cu(Au,Pd) and Au-Ag alloy; (**d**)—stannopalladinite containing the polarite and unnamed phase (Pd,Cu)(As,Sb,Sn) inclusions in the frame of a fine aggregate consisting of zvyagintsevite Pd_3Pb, polarite and Pd_5Pb_3; (**e**)—crystal of stannopalladinite included in tetraferroplatinum in associations with chalcopyrite (Cp) and pentlandite (Pn); (**f**)—microaggregate, consisting of zvyagintsevite, polarite, Au-Ag alloy and chalcopyrite. Data in Tables 6–10.

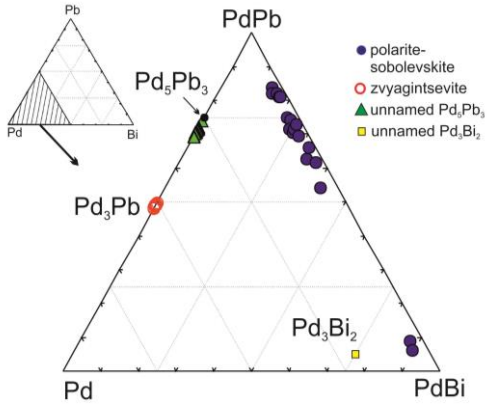

Figure 13. Position of zvyagintsevite, ploarite and sobolevskite from the Southern 2 orebody in the system Pd-PdPb-PdBi.

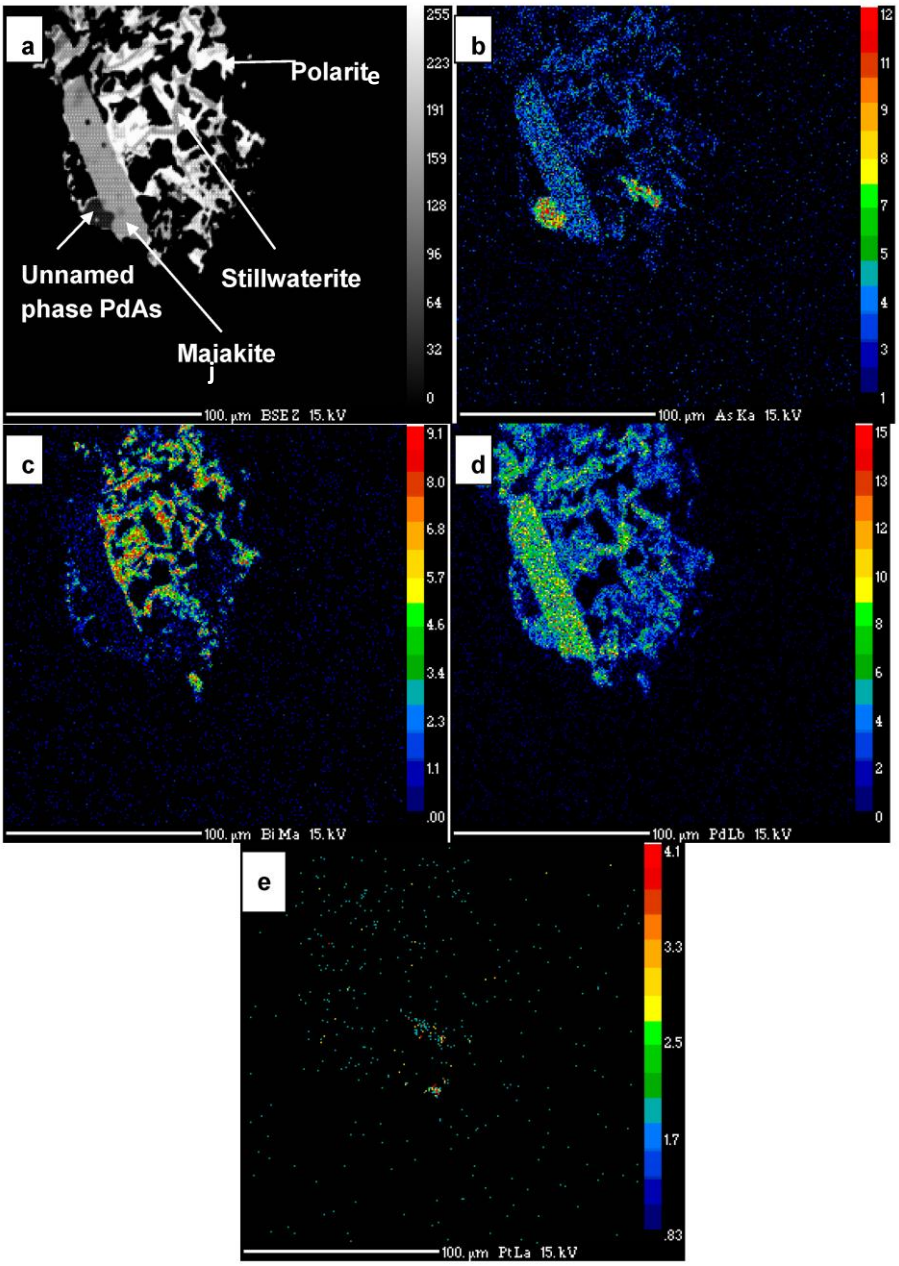

Figure 14. Association of PGE minerals in ore of the Southern 2 orebody. (**a**)—BSE image; (**b**–**e**)—images in the characteristic X-ray radiation: (**b**)—AsKα, (**c**)—BiMα, (**d**)—PdLβ, (**e**)—Pt-Lα.

A large (more than 1 mm) microaggregate of PGM has been studied in detail (Figure 15, Table 11). The euchedral grain of stannopalladinite (points 1 and 2 in Figure 15b) is bordered by the Pd_5Pb_3 phase (points 3 and 4) which is included in stannopalladinite too (points 7) at upper part of the microaggregate. Tetraferroplatinum (points 9–11) is an outer rim after the Pd_5Pb_3 phase. The top most part of this microaggregateis represented by the intergrowth of polarite (white, point 12) with undiagnosed phase due to its small size (as shown in Figure 15g). The outer rim of this intergrovth is composed of a gold-silver alloy in association with zvyagintsevite. The rounded grains of stanopalladinite include zvyagintsevite (point 38), and Pd_5Pb_3 phase localized in interstices of grains in the middle part of the microaggregate (Figure 14d). Tetraferroplatinum is also included in the stannopalladinite grains (point 35) and occur as a rim around them (point 36). The lower part of the PGM cluster is represented by a porous aggregate of Au-Ag alloys containing Cu and Pd in which tetraferroplatinum and stannopalladinite are included.

Of particular interest are the crooked areas in the grain of chalcopyrite enriched with silver. They are located on the contact of chalcopyrite with PGM. Figure 15h shows the different brightness areas due to silver content ranging from 5.74 to 25.96 wt % (points 59–61). The concentration of Ag has a negative correlation with Fe content in this phase with $R^2 = 0.9997$.

Table 11. Chemical composition of platinum group minerals, wt %.

No.	S	Fe	Ni	Cu	Ag	Sn	Pd	Pt	Au	Pb	As	Bi	Total
1				9.0		21.2	56.4	1.2		9.9			99.13 *
2				7.5		21.6	59.6	0.9		10.1			100.84 **
3					3.2		45.7			48.6			97.4
4					1.5		45.8			51.9			99.1
5		18.7	4.2	3.9				75.5					102.3
6					3.9		45.3			48.2			97.4
7					0.2		48.7			51.7			100.6
8							62.4			38.6			100.9
9		17.3	3.5	3.5				72.3					96.6
10		16.8	3.8	3.4				71.2					99.1
11		17.4	3.4	3.2				73.2					97.2
12				0.9			35.2			46.8		17.8	105.6
13							60.8			38.6			99.5
14		0.65		0.94			78.8				18.9		98.3
15	10.2	1.5		2.6	43.8		14.1	0.7	24.1		2.4		99.3
16	8.7	2.4		2.3	52.8		3.8	5.1	27.7		0.9		103.8
17				7.2		19.2	60.5			13.9			100.7
18							61.6			38.5			100.1
19							47.4			49.9			97.2
20					68.1				30.3				98.4
21	33.7	33.2		33.2									101
22		18.0	3.5	2.7				75.7					99.9
23				9.6		20.1	57.8			14.0			101.5
24				9.0		23.1	56.6			11.9			100.6
25					1.8		47.3			50.9			100.0
26				6.1		20.7	59.4			12.6			98.8
27							36.8					63.3	100.0
28				6.3		20.8	61.0			10.9			99.0
29							34.1			46.2		20.8	101.0
30							48.0			51.8			99.8
31							35.8					64.1	99.8
32		18.2	3.1	2.7				75.0					99.0
33				1.3	70.3				26.9				99.6
34		16.8	3.2	3.8			3.6	72.8					100.3
35		17.8	3.5	2.7				76.0					100.0
No.	**S**	**Fe**	**Ni**	**Cu**	**Ag**	**Sn**	**Pd**	**Pt**	**Au**	**Pb**	**As**	**Bi**	**Total**
36		18.3	3.51	4.23				74					100

37						49			51		100
38						45			55		100
39				47.9		8.74	14.5	28.9			100
40				47.7		7.63	11.4	33.3			100
41						62			38		100
42				7.85	21.5	61.3			9.38		100
43						44.9			52.2		97.08
44						60.4			38.6		99.37
45				6.76	20.7	59.3			13.1		99.79
46				6.26	20.7	59.2			13.6		99.79
47						60.4			38.6		99.33
48				6.26	20.7	59.2			13.6		99.79
49		18.5	4.19	2.81			75.8				101.3
50				45.9	6.42	7	11.9	28.2			99.41
51				1.4		44.1			31.4	23.7	100.6
52				0.22		34.2			44.9	18.5	97.72
53				7.23	19.8	59.1			13.6		99.89
54		17.8	3.03	3.81		3.55	72				100.2
55		16.7	3.35	4.01		3.39	72.8				100.3
56						48			51.8		99.82
57				8.58	20.1	57.8			13.9		100.5
59	33.6	29.1		32.7	5.74						101.1
60	26.2	18.5		19.4	26			10.8			101.4
61	33	27.7		31.7	8.63						101

Note. Mineral, Formula: 1: Stannopalladinite, $(Pd_{4.63}Pt_{0.05})_{4.68}(Sn_{1.56}Pb_{0.42}Sb_{0.10})_{2.08}Cu_{1.24}$; 2: Stannopalladinite, $(Pd_{4.85}Pt_{0.04})_{4.89}(Sn_{1.58}Pb_{0.42}Sb_{0.08})_{2.08}Cu_{1.03}$; 3: Unnamaed phase, $(Pd_{4.95}Ag_{0.34})_{5.29}Pb_{2.71}$; 4: Unnamaed phase, $(Pd_{4.95}Ag_{0.16})_{5.11}Pb_{2.89}$; 5: Tetraferroplatinum, $Pt_{0.91}(Fe_{0.78}Ni_{0.17}Cu_{0.14})_{1.09}$; 6: Unnamaed phase, $(Pd_{4.91}Ag_{0.42})_{5.33}Pb_{2.68}$; 7: Unnamaed phase, $(Pd_{5.16}Ag_{0.02})_{5.18}Pb_{2.82}$; 8: Zvyagintsevite, $Pd_{3.04}Pb_{0.96}$; 9: Tetraferroplatinum. $Pt_{0.93}(Fe_{0.78}Ni_{0.15}Cu_{0.14})_{1.07}$; 10: Tetraferroplatinum, $Pt_{0.93}(Fe_{0.77}Ni_{0.17}Cu_{0.14})_{1.08}$; 11: Tetraferroplatinum, $Pt_{0.94}(Fe_{0.79}Ni_{0.14}Cu_{0.14})_{1.06}$; 12: Polarite, $(Pd_{1.01}Cu_{0.04})_{1.05}(Pb_{0.69}Bi_{0.26})_{0.95}$; 13: Zvyagintsevite, $Pd_{3.02}Pb_{0.98}$; 14: Unnamaed phase, $(Pd_{2.90}Cu_{0.06}Fe_{0.05})_{2.95}As_{0.99}$; 15: Polyphase, $(Ag_{0.38}Au_{0.11})_{0.49}(S_{0.29}As_{0.03})_{0.32}(Pd_{0.12}Cu_{0.04}Fe_{0.02})_{0.18}$; 16: Polyphase, $(Ag_{0.46}Au_{0.13})_{0.59}(S_{0.26}As_{0.01})_{0.27}(Fe_{0.04}Cu_{0.03}Pd_{0.03}Pt_{0.02})_{0.12}$; 17: Stannopalladinite, $Pd_{5.00}(Sn_{1.42}Pb_{0.59})_{2.01}Cu_{0.99}$; 18: Zvyagintsevite, $Pd_{3.03}Pb_{0.97}$; 19: Unnamaed phase, $Pd_{2.60}Pb_{1.40}$; 20: Au-Ag alloy, $Ag_{0.80}Au_{0.20}$; 21: Chalcopyrite, $Fe_{1.10}Cu_{0.96}S_{1.94}$; 22: Tetraferroplatinum, $Pt_{0.96}(Fe_{0.79}Ni_{0.15}Cu_{0.10})_{1.04}$; 23: Stannopalladinite, $Pd_{4.67}(Sn_{1.46}Pb_{0.58})_{2.04}Cu_{1.30}$; 24: Stannopalladinite, $Pd_{4.59}(Sn_{1.68}Pb_{0.50})_{2.18}Cu_{1.23}$; 25: Unnamaed phase, $(Pd_{5.03}Ag_{0.19})_{5.22}Pb_{2.78}$; 26: Stannopalladinite, $Pd_{5.02}(Sn_{1.56}Pb_{0.55})_{2.11}Cu_{0.86}$; 27: Sobolevskite, $Pd_{1.07}Bi_{0.93}$; 28: Stannopalladinite, $Pd_{5.09}(Sn_{1.56}Pb_{0.47})_{2.03}Cu_{0.89}$; 29: Polarite, $Pd_{1.00}(Pb_{0.69}Bi_{0.31})_{1.00}$; 30: Unnamaed phase, $Pd_{5.15}Pb_{2.85}$; 31: Sobolevskite, $Pd_{1.05}Bi_{0.95}$; 32: Tetraferroplatinum, $Pt_{0.96}(Fe_{0.81}Ni_{0.13}Cu_{0.11})_{1.05}$; 33: Au-Ag alloy, $Ag_{0.81}Au_{0.17}Cu_{0.03}$; 34: Tetraferroplatinum, $(Pt_{0.91}Pd_{0.08})_{0.99}(Fe_{0.73}Cu_{0.15}Ni_{0.13})_{1.01}$; 35: Tetraferroplatinum, $Pt_{0.96}(Fe_{0.79}Ni_{0.15}Cu_{0.11})_{1.05}$; 36: Tetraferroplatinum, $Pt_{0.91}(Fe_{0.79}Cu_{0.16}Ni_{0.14})_{1.09}$; 37: Zvyagintsevite, $Pd_{2.61}Pb_{1.39}$; 38: Zvyagintsevite, $Pd_{2.46}Pb_{1.54}$; 39: Auricupride, $Cu_{2.85}(Au_{0.55}Pd_{0.31}Pt_{0.28})_{1.14}$; 40: Auricupride, $Cu_{2.86}(Au_{0.64}Pd_{0.27}Pt_{0.22})_{1.13}$; 41: Zvyagintsevite, $Pd_{3.04}Pb_{0.96}$; 42: Stannopalladinite, $Pd_{4.98}(Sn_{1.57}Pb_{0.39})_{1.96}Cu_{1.07}$; 43: Unnamaed phase, $Pd_{5.01}Pb_{2.99}$; 44: Zvyagintsevite, $Pd_{3.01}Pb_{0.99}$; 45: Stannopalladinite, $Pd_{4.94}(Sn_{1.55}Pb_{0.56})_{2.11}Cu_{0.94}$; 46: Stannopalladinite, $Pd_{4.97}(Sn_{1.56}Pb_{0.59})_{2.15}Cu_{0.88}$; 47: Zvyagintsevite, $Pd_{3.01}Pb_{0.99}$; 48: Stannopalladinite, $Pd_{4.97}(Sn_{1.56}Pb_{0.59})_{2.15}Cu_{0.88}$; 49: Tetraferroplatinum, $Pt_{0.93}(Fe_{0.79}Ni_{0.17}Cu_{0.11})_{1.07}$; 50: Auricupride, $(Cu_{1.37}Ag_{0.11})_{1.48}(Au_{0.27}Pd_{0.13}Pt_{0.12})_{0.52}$; 51: Polarite, $Pd_{1.18}Cu_{0.06})_{1.24}(Pb_{0.43}Bi_{0.32})_{0.75}$; 52: Polarite, $(Pd_{1.02}Cu_{0.01})_{1.03}(Pb_{0.69}Bi_{0.28})_{0.97}$; 53: Stannopalladinite, $Pd_{4.93}(Sn_{1.48}Pb_{0.58})_{2.06}Cu_{1.01}$; 54: Tetraferroplatinum, $(Pt_{0.89}Pd_{0.08})_{0.97}(Fe_{0.77}Cu_{0.14}Ni_{0.12})_{1.03}$; 55: Tetraferroplatinum, $(Pt_{0.91}Pd_{0.08})_{0.99}(Fe_{0.73}Cu_{0.15}Ni_{0.14})_{1.02}$; 56: Unnamaed phase, $Pd_{5.15}Pb_{2.85}$; 57: Stannopalladinite, $Pd_{4.75}(Sn_{1.48}Pb_{0.59})_{2.07}Cu_{1.18}$; 59: Ag-chalcopyrite, $Fe_{0.97}Cu_{0.96}S_{1.96}Ag_{0.10}$; 60: Ag-chalcopyrite, $Fe_{0.76}Cu_{0.70}S_{1.87}(Ag_{0.55}Au_{0.13})_{0.68}$; 61: Ag-chalcopyrite, $Cu_{0.95}Fe_{0.94}S_{1.96}Ag_{0.15}$.

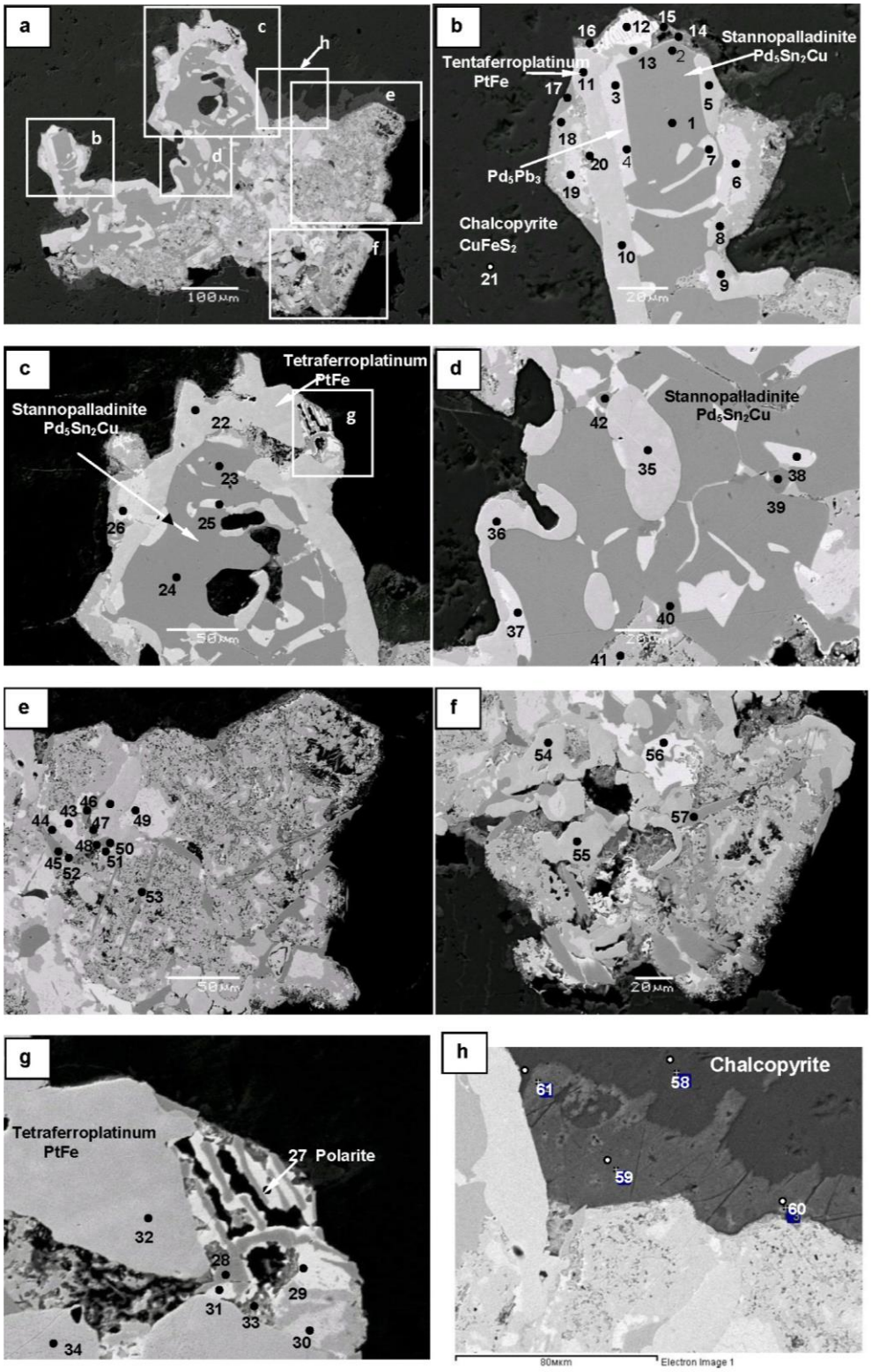

Figure 15. Microaggregate of PGM in chalcopyrite. BSE images. Points are correspond to N analyses in Table 11. (**a**)—positios of photos given in figures **b**–**h**; (**b**)—rim of Pd_5Pb_3 and tetraferroplatinum around stannopalladinite, (**c**)—rim of tetraferroplatinum around stannopalladinite, (**d**)—aggragate of stannopalladinite with tetraferroplatinum and zvyagintsevite inclusions, (**e**)—microporous agraggate of platinum-group minerals with stannopalladinite and tetraferroplatinum crystals, (**f**)—stannopalladinite, tetraferroplatinum and Pd_5Pb_3 grains in microporous agraggate of platinum-group minerals, (**g**)—rims of polarite on stannopalladinite, (**h**)—Ag-bearing chalcopyrite on the aggragate of platinum-group minerals.

5. Discussion

The origin of the Norilsk deposits assumes two stages of their formation: The appearance of the sulfide phase in the melt and its further evolution and crystallization. In this paper, we consider only the second aspect of genesis, namely, the structural position of the magmatic and sulfide bodies and possible mechanism of the formation of massive ores from an already existed sulfide melt.

The Norilsk-Kharaelakh Fault was the main structure which controlled the magmas intrusion, their localization and position of the orebodies. First of all, different magma portions ascended from the deep zones to the modern chambers using this large fracture. There were at least three pulses of the magma intrusions that formed three branches: North-Eastern, North-Western and South-Western. Their rear parts are located in the Norilsk-Kharaelakh Fault, while the heads are stretched in the Northern, Western and Eastern directions, respectively (Figure 2). The most complex structure is typical of the South-Western branch, due to the melt entered into the block, restricted by the branches of this major disturbance. Their steep fall to the center of the graben determined the steep inclination of the sides of the South-Western body. Contacts of the other two intrusive branches are more flat. During the cooling of the silicate melt contractile cracks were formed, they were located subparallel to the steeply sloping sides.The main part of the sulfide melt was concentrated inside these cracks. The cracks in the North-Western and North-Eastern branches occur a subhorizontal position, and the massive ores are subhorizontal as well. Thus, the position of the massive ores of the Talnakh deposit was largely determined by the prototectonics of the territory. The Norilsk-Kharaelakh Fault was a long-lived structure, because significant displacements along its branches and feathering cracks occurred after the crystallization of silicate and sulfide melts. As a result, the South-Western branch was shifted not only relative to the North-Eastern and North-Western branches, but it was also subdivided into the separate blocks (Figure 3, II-II cross-section). The Southern part of the Southern 2 orebody was descended at 40 m compared to the Northern one (Figure 7b, VI-VI cross-section).

The Southern 2 orebody composition supports our conclusion that the branches of the Talnakh intrusion were formed from different portions of the silicate melt, which carried a different sulfide melt. The silicate part of these branches were similar (Figure 6) while the sulfide melts were different: In the South-Western branch the sulfide melt was enriched with Cu and PGE in comparison with the melts of the North-Eastern and North-Western branches. The structure of the South-Western branch and the fundamental difference in the composition of ores indicate that the disturbances into the portions took place before intrusion of the magmas. We cannot estimate the time relationship of the intrusive branches, but it is likely that they were formed sequentially, from magmas flowing out of the one channel.

So far, two hypotheses of massive ore origin for the Norilsk-Talnakh ores have been suggested: they were formed either as a result of the intrusion of an independent portion of the sulfide melt [18,19], or as a result of filter pressing processes when the sulfide melt penetrated into the host rocks.

The last model was elaborated in detail by Likhachev [5,8], who demonstrated the pipe-like structure of the intrusive body based on the numerous cross-sections of the North-Western branch of the Talnakh intrusion. The bodies of massive ores are localized under the deflection of the massif bottom sole (Figure 16). The same position of massive ore is also visible in the distribution of ore bodies and isopaches of the Talnakh intrusion, shown in Figure 2. Indeed, the bodies of massive ores are confined to the areas of maximum intrusion thickness. Based on the study of the orientation of olivine crystals in rocks, Likhachev [6,8] proposed an explanation of this fact. At the narrowed and enlarged sections of the intrusion chamber (with a difference in the cross-sectional area), the nature of the flow varies from turbulent to laminar. With the settling of crystals from magma with laminar flow, a planar orientation of the grains relative to the bottom is formed, while with settling from turbulent flow, a non-oriented grain orientation is observed. The study of the crystals' distribution made it possible to conclude that the subsidence of the bulk of the crystals and sulfides settles due to a change in the flow velocity from the narrowed towards the extended sections. Thus, there is a correlation between the thicknesses of disseminated and massive ores in the bottom sagging. Sulfides,

penetrated into the host rocks under the intrusion, formed massive ores. A similar picture arises when considering the Kharaelakh branch. Likhachev [8] concluded that the main deposit of the Oktyabr'skoe deposit was formed as a result of the introduction of sulfides with different portions of the melt into the same place. Conclusions on the formation of the Talnakh deposits from different portions of magma were also made by Stekhin [46].

In the South-Western branch, the structure of the intrusion and associated mineralization is fundamentally different: the orebodies are confined to steep fractures in the endocontact of the intrusive body. Consequently, the sulfide melt did not penetrateinto the host rocks during the silicate crystallization, as described above, but was concentrated in compression fractures and faults. The mechanism of its concentration basically remained the same (filter-pressing), but the morphology of orebodies changed due to other tectonic conditions and the composition of the surrounding rocks. Different types of morphologies of ores, depending on the physical properties of rocks, were modeled by Saumur and Cruden [70].

The formation of the Southern 2 orebody from a high-copper sulfide melt remains an open question. Usually such a composition is considered as a residual sulfide melt formed during crystallization and moved some distance from the place of its crystallization [8]. In this case, at first, the higher-temperature pyrrhotite melt crystallized and stayed in place, while the chalcopyrite melt moved. However, this scenario is possible only after the crystallization of the silicate melt. In this case, the disseminated ores have a chalcopyrite-pyrrhotite composition. However, the main conclusion of our study is that the melt did not migrate through fractures over long distances. It was formed in situ, confirmed by the composition of the disseminated ores accompanying the Southern 2 orebody: they are also enriched in copper and platinum metals and consist of the same Cu minerals (chalcocite, bornite) that are absent in other orebodies of the Norilsk-Talnakh region. This indicates that silicate melt carried out Cu-rich sulfide melt from the deep zone; it did not enter the place from outside.

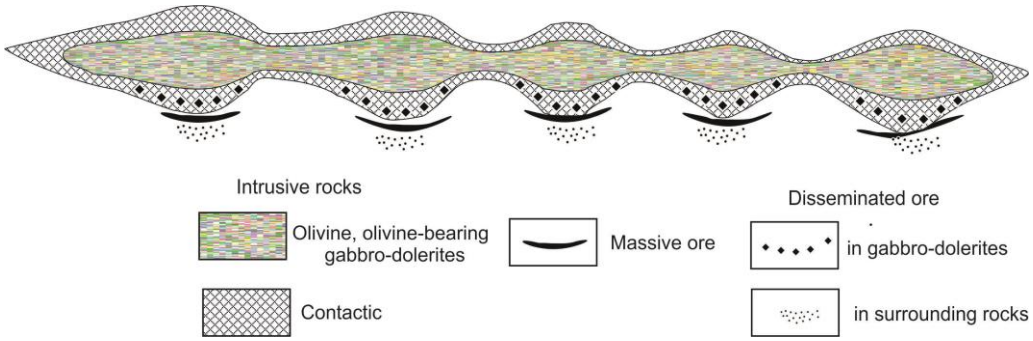

Figure 16. Model of positions of disseminated and massive ore in the North-Western branch of the Talnakh intrusion (after Likhachev [8], with changes).

The mineral composition of the Southern 2 deposit also confirms that it crystallized under physical and chemical parameters that differed from those of the main deposit of the Oktyabr'skoe deposit (higher f_{S2}).

Most of the PGE minerals were previously found in other disseminated, veinlet-disseminated and massive ores of the Norilsk-Talnakh region [51,53,55,58,59,71–74]. All minerals were enriched in copper due to its crystallization from Cu-rich melt. However, the ratio of mineral species and the geochemistry of most of them (minor elements) from sulfides of the Southern 2 orebody have a number of distinctive features. Minerals of Pt predominate over Pd minerals in disseminated ores of all ore occurrences of the Norilsk ore deposits, such as isoferroplatinum, sperrylite, cuperite, moncheite and rustenburgite (from 50% to 80% in different ore occurrences) [75]. These platinum minerals also predominante as in massive ores of different composition and in the placer of the Medvezhy Creek [76], while the Pt minerals are in a subordinate amount (16%) (Figure 11) in the chalcopyrite ores of the Southern 2 orebody of the Talnakh intrusion. They are mainly represented

by tetraferroplatinum and rustenburgite (rare). Typical platinum minerals of the Norilsk ores (isoferroplatinum, sperrylite and cooperite) were not found in the Southern 2 orebody.

6. Conclusions

1. The South-Eastern branch of the Talnakh intrusion is characterized by a specific structure of silicate and sulfide bodies. The tectonic fractures and faults determined their morphology: the intrusion sides and veins of massive ore fall at steep angle to the center in contrast to other massive ore which take a horizontal position.

2. Ore composition of the Southern 2 orebody differs from the composition of other massive ores including the Cu-rich main body of the Octyabr'skoe deposit. It is characterized by high Cu and PGE (ΣPt + Pd = 278 ppm) and specific mineralogical composition: chalcopyrite associates with chalcocite and bornite in massive and also as in disseminated ore. This is evidence of the formation of massive ore in situ, without displacement along the intrusion's contact.

3. PGE minerals contain Cu as impurity. Many minerals widespread in the Norilsk ore were not found in the Southern 2 orebody, they are isoferroplatinum, sperrylite and cooperite.

4. The South-West branch of the Talnakh intrusion and related ore crystallized from separate portion of the silicate melt combined with a Cu-rich sulfide melt.

Acknowledgments: Authors thank the geologists of Ltd. Norilskgeologia S.G. Snisar and S.P. Erykalov for their help with sampling and A. Lebedev, I. Fomin, and E. Krasnova for assistance with field work. We are also grateful to M.R. Nesterenko for her help with study of samples from the borehole SF-10 and N.N. Kononkova for analyses of ore-forming minerals using a Cameca SX-100. This study was supported by Russian Foundation for Basic Research (project No. 16-05-00945).

Author Contributions: N.K. stydied ores in boreholes and undeground mines, wrote the text; N.T. studied ore minerals and constructed diagrams, T.K. constructed map and cross-sections; K.N. did sampling of orebodies on field trip an constructed cross-sections; B.G. studied cores of boreholes, interpreted the analyses of rock geochemistry; I.K., O.T. analysed ores, gave their interpretation, did method discription; L.M. and E.K. studied ore minerals, including platinum-group minerals; Y.B. and A.Y. analysed rocks.

Conflicts of Interest: The authors declare no conflict of interest.

References

1. Sotnikov, A.A. *About Exploration of the Norilsk (Dudinsky) Coal and Copper Deposit in Term of Creating of Northern Marine Route*; Gubernsky typography: Tomsk, Russia, 1919; p. 54. (In Russian)
2. Godlevsky, M.N. *Traps and Ore-Bearing Intrusions of the Norilsk District*; Gosgeoltekhizdat: Moscow, Russia, 1959; p. 61.
3. Godlevsky, M.N.; Likhachev, A.P. Types and distinctive features of ore-bearing formations of copper-nickel deposits. In *Geology and Metallogeny of Copper Deposits*; Nauka: Moscow, Russia, 1984; pp. 124–134.(In Russian)
4. Likhachev, A.P. The Role of Leucocratic Gabbro in the Origin of Norilsk Differentiated Intrusions. *Izv. Akad. Nauk SSSR Ser. Geol.* **1965**, *12*, 50–66. (In Russian)
5. Likhachev, A.P. Ore-bearing intrusions of the Noril'sk region. In *Proceedings of the Sudbury-Noril'sk Symposium*; Ontario Geological Survey: Sudbury, ON, Canada, 1994; pp. 185–201.
6. Likhachev, A.P. The Kharaelakh intrusion and its PGM-Cu-Ni ores. *Rudy and Metals* **1996**, *3*, 48–62. (In Russian)
7. Likhachev, A.P. Trap magmatism and Platinum-Copper-Nickel ore mineralization in the Norilsk District.*Otech. Geol.* **1997**, *10*, 8–19 (In Russian)
8. Likhachev, A.P. *Platinum-Copper-Nickel and Platinum Deposits*; Eslan: Moscow, Russia, 2006; p. 496.
9. Dodin, D.A.; Batuev B.N. Geology and petrology of the Talhakh differentiated intrusions and their metamorphic aureole. In *Petrology and Ore Resource Potential of the Talnakh and Norilsk Differentiated Intrusions*. Nedra: Leningrad, Russia, 1971; pp. 31–100. (In Russian)
10. Zolotukhin, V.V. Trap Magmatism and Formation Conditions of Ore-Bearing Differentiated Intrusions of the Siberian Platform. In *Traps of the Siberian Platform and Their Metallogeny*; Institut zemnoi Kory: Irkutsk, Russia, 1971; pp. 53–59.(In Russian)

11. Zotov, I.A. *The Genesis of Trap Intrusions and Metamorphic Rocks of Talnakh*; Nauka: Moscow, Russia, 1979; p. 187. (In Russian)
12. Zotov, I.A. *Transmagmatic Fluids in Magmatism and Ore Mineralization*; Nauka: Moscow, Russia, 1989; p. 213. (In Russian)
13. Ryabov, V.V. About composition of upper horizons of the Norilsk intrusions with rich chromite mineralization. In *Criteria of ore Potential of Magmatic Rocks*; Nauka: Novosibirsk, Russia, 1984; pp. 124–142. (In Russian)
14. Ryabov, V.V. *Olivines from Norilsk Intrusions as Criteria of Petrogeneses and Ore Producing Process*; Nauka: Novosibirsk, Russia, 1992; p. 182. (In Russian)
15. Ryabov, V.V.; Tsimbalist, V.G.; Yakobi, I.Y. About PGE and chromium concentrations in the upper zones of the Norilsk intrusions. *Doclady Earth Sci.* **1982**, *266*, pp. 466–469. (In Russian)
16. Ryabov, V.V.; Shevko, A.Y.; Gora, M.P. *Igneous Rocks of the Norilsk District. V.1. Petrology of Traps*; Nonparel: Novosibirsk, Russia, 2000; Volume 1–2. (In Russian)
17. Ryabov, V.V., Shevko, A.Y., Gora, M.P. *Trap Magmatism and Ore Formation in the Siberian Norilsk Region Nederland*; Springer: New York, NY, USA, 2014; Volume 1–2.
18. Dyuzhikov, O.A.; Distler, V.V.; Strunin, B.M.*Geology and Ore Potential of the Norilsk Ore District*; Nauka: Moscow, Russia, 1988; p. 248.
19. Dyuzhikov, O.A., Distler, V.V., Strunin, B.M., Mkrtychyan, A.K., Sherman, M.L., Sluzhenikin, S.F., Lurye, A.M. *Geology and Metallogeny of Sulfide Deposits Norilsk Region USSR*; PUBCO: Cleveland, OH, USA, 1992; p. 241.
20. Distler, V.V.; Grokhovskaya, T.L.; Evstigneeva, T.L.; Sluzhenikin, S.F.; Filimonova, A.A.; Dyuzhikov, O.A. *Petrology of Magmatic Sulfide Ore Formation*; Nauka: Moscow, Russia, 1988; p. 232. (In Russian)
21. Naldrett, A.J. A model for the Ni-Cu-PGE Ores of the Norilsk Region and Its Application to Other Areas of Flood Basalts. *Econ. Geol.* **1992**, *87*, 1945–1962.
22. Naldrett, A.J. *Magmatic Sulphide Deposits: Geology, Geochemistry and Exploration*; Springer: Berlin/Heidelberg, Germany; New York, NY, USA, 2004; p. 727.
23. Krivolutskaya, N.A.; Ariskin, A.A.; Sluzhenikin, S.F.; Turovtsev, D.M. Geochemical thermometry of rocks of the Talnakh Intrusion: Assessment of the melt composition and the crystallinity of the parental magma. *Petrology* **2001**, *9*, 389–414.
24. Krivolutskaya, N.A.; Sobolev, A.V.; Snisar, S.G. Mineralogy, geochemistry and stratigraphy of the Maslovsky Pt-Cu-Ni sulfide deposit, Norilsk Region, Russia: Implications for relatioship of ore-bearing intrusions and lavas. *Miner. Depos.* **2012**, *47*, 69–88.
25. Lightfoot, P.C.; Zotov, I.A. Geological relationships between intrusions, country rocks and Ni-Cu-PGE sulfides of the Kharaelakh intrusion, Norilsk region: Implication for the role of sulfide differentiation and metasomatism in their genesis. *Northwest. Geol.* **2014**, *47*, 1–34.
26. Malich, K.N.; Latypov, R.M. Re-Os and S isotope constraints on timing and source heterogeneity of PGE-Cu-Ni sulfide ores: A case study at the Talnakh ore junction, Norilsk province, Russia. *Can. Miner.* **2011**, *49*, 1653–1677.
27. Malitch, K.N.; Belousova, E.A.; Griffin, W.L.; Badanina, I.Y.; Pearson, N.J.; Presnyakov, S.L.; Tuganova, E.V. Magmatic evolution of the ultramafic–mafic Kharaelakh intrusion (Siberian Craton, Russia): Insights from trace-element, U-Pb and Hf-isotope data on zircon. *Contrib. Miner. Pet.* **2010**, *159*, 753–768.
28. Malitch, K.N.; Belousova, E.A.; Griffin, W.L.; Badanina, I.Y. Hafnium-neodymium constraints on source heterogeneity of the economic ultramafic-mafic Norilsk-1 intrusion (Russia). *Lithos* **2013**, *164–167*, 36–46.
29. Malitch, K.N.; Badanina, I.Y.; Puchkov, V.N.; Belousova, E.A.; Stepashko,A.A. Results of U-Pb dating of zircons from wehrlite of the platinum-bearing Feklistov massif (Shantar Archipelago, Russia).*Dokl. Earth Sci.* **2017**, *475*, 762–765. doi:10.1134/S1028334X17070248.
30. Malitch, K.N.; Belousova, E.A.; Griffin, W.L.;Badanina, I.Y.;Latypov, R.S.; Sluzhenikin, S.F. Chapter 7—New insights on the origin of ultramafic-mafic intrusions and associated Ni-Cu-PGE sulfide deposits of the Norilskand Taimyr provinces, Russia:Evidence From Radiogenic- And Stable-Isotope Data. In *Processes and Ore Deposits of Ultramafic-Mafic Magmas through Space and Time*; Mondal, S., Griffin, W.L., Eds.; Elsevier Inc.: Amsterdam, The Netherlands, 2017; pp. 197–238.

31. Sluzhenikin, S.F.; Krivolutskaya, N.A.; Rad'ko, V.A.; Malitch, K.N.; Distler, V.V.; Fedorenko, V.A. *Ultramafic-Mafic Intrusions, Volcanic Rocks and PGE-Cu-Ni Sulfide Deposits of the Norilsk Province, Polar Siberia Field Trip Guidebook*; Zavaritsky Institute of Geology and Geochemistry of the Ural Branch (UB) of the Russian Academy of Sciences (RAS): Yekaterinburg, Russia, 2014; p. 87.
32. Spiridonov, E.M. The ore-magmatic system of the Norilsk ore field. *Rus. Geol. Geophys.* **2010**, *51*, 1059–1077.
33. Spiridonov, E.M.; Kulagov, E.A.; Serova, A.A.; Kulikova, I.M.; Korotaeva, N.N.; Sereda, E.V.; Tushentsova, I.N.; Belova, S.N.; Zhukov, N.N. Genetic mineralogy of Pd, Pt, Au, Ag, and Rh at the Norilsk sulfide ores. *Geol. Ore Depos.* **2015**, *57*, 382–402.
34. Krivolutskaya, N.A. *Siberian Traps and Pt-Cu-Ni Deposits in the Norilsk Area*; Springer: Amsterdam, The Netherlands, 2016; p. 361.
35. Malitch, K.N.; Khiller, V.V. Results of chemical dating of monazite from the Talnakh economic intrusion.*Dokl. Earth Sci*. **2017**, *474*, 565–568. doi:10.1134/S1028334X17050130.
36. Kamo, S.L.; Czamanske, G.K.; Amelin, Y.A. Rapid eruption of Siberian flood-volcanic rocks and evidence for coincidence with the Permian-Triassic boundary and mass extinction at 251 Ma. *Earth Plan. Sci. Lett.* **2003**, *214*, 75–91.
37. Burgess, S.D.; Bowring, S.A. High-precision geochronology confirms voluminous magmatism before, during, and after Earth's most severe extinction. *Sci. Adv.* **2015**, *1*, e1500470.
38. Zolotukhin, V.V.; Ryabov, V.V.; Vasil'ev, Y.R.; Shatkov V.A. *Petrology of the Talnakh Ore-Bearing Differentiated Trap Intrusion*; Nauka: Novosibirsk, Russia, 1975; p. 425.(In Russian)
39. Rad'ko, V.A. Model of dynamic differentiation of intrusive traps at the northwestern siberian trap. *Geol. Geophys.***1991**, *32*, 19–27. (In Russian)
40. Rad'ko,V.A. *Facies of Intrusive and Volcanic Magmatism in the Norilsk District*; Map-Making Department at VSEGEI: St. Petersburg, Russia, 2016; p. 285. (In Russian)
41. Li, C.; Ripley, E.M.; Naldrett, A.J. A new genetic model for the giant Ni-Cu-PGE sulfide deposits associated with the Siberian flood basalts. *Econ. Geol.* **2009**, *104*, 291–301.
42. Le Vaillant, M.; Barnes, S.J.; Mungall, J.E.; Mungall, E.L. Role of degassing of the Norilsk nickel deposits in the Permian-Triassic mass extinction event. *PNAS* **2017**, *114*, 2485–2490.
43. Genkin, A.D.; Distler, V.V.; Gladyshev, G.D.; Filimonova, A.A.; Evstigneeva, T.L.; Kovalenker, V.A.; Laputina, I.P.; Smirnov, A.V.; Grokhovskaya, T.L. *Sulfide Copper–Nickel Ores of the Norilsk Deposits*; Nauka: Moscow, Russia, 1981; p. 374.
44. Sukhanova, E.N. Zoning of orebodies, intrusions, and tectonomagmatic clusters and its applied implications. In *Geology and Mineral Resources of the Norilsk Mining District*; NTO Tsvetmet: Norilsk, Russia, 1968; pp. 139–142. (In Russian)
45. Torgashin, A.S. Geology of the massive and copper ore of the Western part of the Octyabr'sky deposit. In *Proceeding of the Norilsk-Sudbury Symposium*; Ontario Geological Survey: Sudbury, ON, Canada, 1994; pp. 231–242.
46. Stekhin, A.I. Mineralogical and geochemical characteristics of the Cu-Ni ores of the Oktyabr'skoe and Talnakh deposits. In *Proceeding of the Norilsk-Sudbury Symposium*; Ontario Geological Survey: Sudbury, ON, Canada, 1994; pp. 231–242.
47. Distler, V.V. Platinum Mineralization of the Norilsk Deposits, Proceeding of the Sudbury-Norilsk Symposiun. *Sudbury Spec.* **1994**, *5*, 243–260.
48. Naldrett, A.J.; Fedorenko, V.A.; Asif, M., Lin, S.; Kunilov, V.E.; Stekhin, A.I.; Lightfoot, P.C.; Gorbachev, N.S. Controls on the composition of Ni-Cu sulfide deposits as illustrated by those at Norilsk, Siberia. *Econ. Geol.* **1996**, *91*, 751–773.
49. Duran, C.J.; Barnes, S.J.; Pleše, P.; Kudrna Prašek, M.; Zientek, M.L.; Pagé P. Fractional crystallization-induced variations in sulfides from the Norilsk-Talnakh mining district (polar Siberia, Russia). *Ore Geol. Rev.* **2017**, *90*, 326–351.
50. Budko, I.A.; Kulagov, E.A. New mineral talnakhite—Cubic spice of chalcopyrite. *Zap. Vses. Min. Soc.* **1968**, *97*, 27–32. (In Russian)
51. Genkin, A.D. *Minerals of Platinum Metals in Ores of the Norilsk 1 Deposit*; Nauka: Moscow, Russia, 1968; p. 106. (In Russian)
52. Genkin, A.D.; Evstigneeva, T.L. Associations of platinum-group minerals of theNorilsk copper-nickel sulfide ores. *Econ. Geol.* **1986**, *81*, 1203–1212.

53. Genkin, A.D.; Evstigneeva, T.L.; Troneva, N.V.; Vyal'sov, L.P. Polyarite—New mineral from copper-nickel sulfide ores. *Zap. Vses. Min. Ob.* **1969**, *98*. (In Russian)
54. Genkin, A.D.; Evstigneeva, T.L.; Troneva, N.V.; Vyal'sov, L.P. Mayakite—PdNiAs—New mineral from copper-nickel sulfide ores. *Zap. Vses. Min. Soc.* **1976**, *105*, 201–206. (In Russian)
55. Begizov, V.D.; Meshankina, V.I.; Dubakina, L.S. Palladoarsenide Pd2As—New natural arsenide of Pd from copper-nickel ores of the Oktyabr'skoe deposit. *Zap. Vses. Min. Ob. Ch. 103* **1974**, *1*, 104–107. (In Russian)
56. Kovalenker, V.A.; Laputina, I.P.; Vyalsov, L.N.; Genkin, A.D.; Evstigneeva, T.L. Tellurium minerals in the sulphide copper-nickel ores of the Talnakh and Oktyabrsky deposits (Norilsk region). *Proc. Acad. Sci. USSR A Ser. Geol.* **1972**, *1*, 85–97. (In Russian)
57. Kovalenker, V.A.; Genkin, A.D.; Evstigneeva, T.L.; Laputina, I.P. Telargpalite—New mineral of Pd, Ag, and Te from Cu-Ni ores of the Oktyabr'skoe deposit. *Zap. Min. Soc.* **1974**, *5*, 5–6. (In Russian)
58. Evstigneeva, T.L.; Genkin, A.D.; Kovalenker, V.A. New mineral of Bi and Pd—Sobolevskite and nomenclature of minerals from system PdBi-PdTe-PdSb. *Zap. Vses. Min. Ob. Ch. 104* **1975**, *5*. (In Russian)
59. Spiridonov, E.M.; Kulagov, E.A.; Kulikova, I.M. Platinum and palladium-bearing tetraauricupride and associated minerals in the ores of the Norilsk-I deposit. *Geol. Ore Depos.* **2003**, *45*, 261–271. (In Russian)
60. Spiridonov, E.M.; Kulagov, E.A.; Kulikova, I.M. Association of minerals of palladium, platinum and gold in ores of the Norilsk deposit. *Geol. Ore Depos.* **2004**, *46*, 175–192. (In Russian)
61. Spiridonov, E.M.; Korotaeva, N.N.; Kulikova, I.M.; Mashkina, A.A.; Zhukov, N.N. Palladoarsenide Pd2As—A breakdown product of majakite PdNiAs in the Norilsk sulfide ores. *New Data Min. Fersm. Mus. RAS* **2011**, *46*, 48–54. (In Russian)
62. Sluzhenikin, S.F.; Mokhov, A.V. Gold and silver in PGE-Cu-Ni and PGE ores of the Norilsk deposits, Russia. *Min. Depos.* **2015**, *50*, 465–492, doi:10.1007/s00126-014-0543-2.
63. *The Geological Map of the Norilsk Area*; Strunin, Ed.; VSEGEI: St-Peterburg, Russia, 1994. (In Russian)
64. *The Legend for 1: 50,000 Scale Map, Norilsk Group*; Lul'ko, V.A., Ed.; Geoinformmark: Moscow, Russia, 1993; p. 79. (In Russian)
65. Natorkhin, I.A.; Arkhipova, A.I.; Batuev, B.N. *Petrology of the Talnakh Intrusions*; Nedra: Leningrad, Russia, 1977; p. 236. (In Russian)
66. Turovtsev, D.M. *Contact Metamorphism of the Norilsk Intrusions*; Nauchny Mir: Moscow, Russia, 2002; p. 293. (In Russian)
67. Zen'ko, T.E.; Czamanske, G.K. Special and petrologic aspects of the Norilsk and Talnakh ore junctions. In *Proceedings of the Sudbury-Norilsk Symposium*; Ontario Geological Survey: Sudbury, ON, Canada, 1994; pp. 263–282.
68. Czamanske, G.K.; Zen'ko, T.E.; Fedorenko, V.A. Petrographic and Geochemical Characterization of Ore-Bearing Intrusions of the Norilsk Type, Siberia; With Discussion of Their Origin. *Res. Geol. Spec.* **1995**, *18*, 1–45.
69. Lyul'ko, V.A.; Fedorenko, V.A.; Distler, V.V.; Sluzhenikin, S.F. Geology and Ore Deposits of the Norilsk Region; In *Guidbook of VII International Platinum Symposium*; Moskovsky contact Press: Moscow, Russia, 1994; p. 67.
70. Saumur, B.M.; Cruden, A.R. Ore Ingress of magmatic Ni-Cu sulphide liquid into surrounding brittle rocks: Physical & structural controls. *Ore Geol. Rev.* **2017**, *90*, 439–445.
71. Sluzhenikin, S.F.; Distler, V.V.; Dyuzhikov, O.A.; Kravtsov, V.F.; Kunilov, V.E.; Laputina, I.P.; Turovtsev, D.M. Low-sulfide platinum mineralization in the Norilsk differentiated intrusions. *Geol. Ore Depos.* **1994**, *36*, 195–217. (In Russian)
72. Sluzhenikin, S.F.; Mokhov, A.V. Natural iron-platinum, palladium-platinum and palladium-copper alloys in platinum-copper-nickel and platinum ores of the Norilsk deposit. In *Problems of Ore Geology, Mineralogy, Petrology and Geochemistry*; Abstract: Moscow, Russia, 2008; pp. 346–347. (In Russian)
73. Distler, V.V.; Sluzhenikin, S.F.; Cabri, L.J.; Krivolutskaya, N.A.; Turovtsev, D.M.; Golovanova, T.A.. Platinum ores of the Norilsk layered intrusions: the proportion of the magma and fluid concentration. *Geol. Ore Depos.* **1999**, *41*, 241–265.
74. Sluzhenikin, S.F.; Mokhov, A.V. *Minerals of System PdBi-PdTe-PdSb-PdPb in Pt-Cu-Ni and Pt Ores of the Norilsk Region*; Annual session of RMO: Moscow, Russia, 2007; pp. 119–121. (In Russian)

75. Komarova, M.Z.; Kozyrev, S.M.; Simonov, O.N.; Lyul'ko, V.A. The PGE mineralization of disseminated sulfide ores of the Norilsk-Taimyr Region.In *The Geology, Geochemistry, Nineralogy and Mineral Beneficiation of Platinum-Group Elements*; Cabri, L.J., Ed.; Canadian Institute of Mining, Metallurgy and Petroleum: Montreal, QC, Canada, 2002; Volume 54, pp. 547–567.
76. Kozyrev, S.M.; Komarova, M.Z.; Emelina, L.N.; Oleshkevich, O.I.; Yakovleva, O.A.; Lyalinov, D.V.; Maximov, V.I. The Mineralogy and Behaviour of PGM During Processing of the Norilsk-Talnakh PGE-Cu-Ni Ores. In *The Geology, Geochemistry, Nineralogy and Mineral Beneficiation of Platinum-Group Elements*; Cabri, L.J., Ed.; Canadian Institute of Mining, Metallurgy and Petroleum: Montreal, QC, Canada, 2002; Volume 54, pp. 757–791.